GENETICS

MARCH 2018 • VOLUME 208 • ISSUE 3

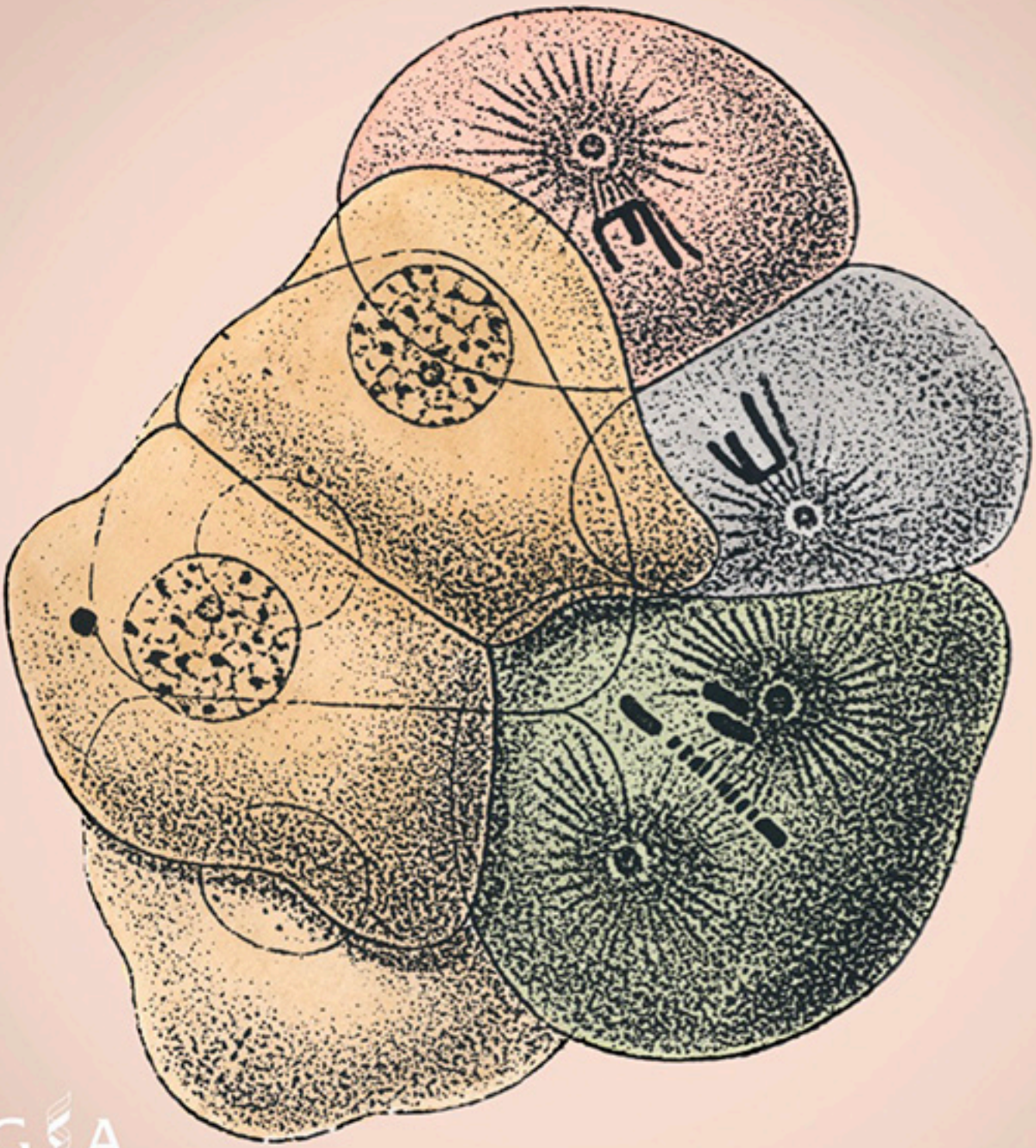

GSA
Genetics Society of America

A CRISPR Tagging-Based Screen Reveals Localized Players in Wnt-Directed Asymmetric Cell Division

Jennifer K. Heppert,* Ariel M. Pani,*,† Allyson M. Roberts,‡ Daniel J. Dickinson,*,†,1 and Bob Goldstein*,†,‡,2

*Department of Biology, †Lineberger Comprehensive Cancer Center, and ‡Curriculum in Genetics and Molecular Biology, University of North Carolina at Chapel Hill, North Carolina 27599

ABSTRACT Oriented cell divisions are critical to establish and maintain cell fates and tissue organization. Diverse extracellular and intracellular cues have been shown to provide spatial information for mitotic spindle positioning; however, the molecular mechanisms by which extracellular signals communicate with cells to direct mitotic spindle positioning are largely unknown. In animal cells, oriented cell divisions are often achieved by the localization of force-generating motor protein complexes to discrete cortical domains. Disrupting either these force-generating complexes or proteins that globally affect microtubule stability results in defects in mitotic positioning, irrespective of whether these proteins function as spatial cues for spindle orientation. This poses a challenge to traditional genetic dissection of this process. Therefore, as an alternative strategy to identify key proteins that act downstream of intercellular signaling, we screened the localization of many candidate proteins by inserting fluorescent tags directly into endogenous gene loci, without overexpressing the proteins. We tagged 23 candidate proteins in *Caenorhabditis elegans* and examined each protein's localization in a well-characterized, oriented cell division in the four-cell-stage embryo. We used cell manipulations and genetic experiments to determine which cells harbor key localized proteins and which signals direct these localizations *in vivo*. We found that Dishevelled and adenomatous polyposis coli homologs are polarized during this oriented cell division in response to a Wnt signal, but two proteins typically associated with mitotic spindle positioning, homologs of NuMA and Dynein, were not detectably polarized. These results suggest an unexpected mechanism for mitotic spindle positioning in this system, they pinpoint key proteins of interest, and they highlight the utility of a screening approach based on analyzing the localization of endogenously tagged proteins.

KEYWORDS asymmetric cell division; CRISPR; development; dynein; Wnt signaling

ORIENTED cell divisions are essential for generating cellular diversity and maintaining tissue architecture during development and later, as cells proliferate in established tissues. The position of the mitotic spindle within a dividing cell determines the orientation of division (Rappaport 1961; di Pietro *et al.* 2016), and both intracellular and extracellular cues are known to influence mitotic spindle positioning. In some cases, signals from neighboring cells are important spatial cues for directing mitotic spindle orientation (Goldstein 1995b; Siller and Doe 2008; Gillies and Cabernard 2011; Werts and Goldstein 2011; Williams *et al.* 2011; Smith *et al.* 2017). Evidence from a short, but growing, list of systems has provided some insight into how signaling between cells directs mitotic spindle positioning (Le Grand *et al.* 2009; Inaba *et al.* 2010; Ségalen *et al.* 2010; Werts *et al.* 2011; Yoshiura *et al.* 2012; Habib *et al.* 2013; Delaunay *et al.* 2014; Xia *et al.* 2015). Although signaling molecules play well-established roles in regulating proliferation and cell fate, how they function mechanistically to orient cell divisions is less well understood.

During oriented cell divisions, polarity cues direct the local enrichment of force-generating complexes at specific regions of the cell cortex (reviewed in di Pietro *et al.* 2016). These force-generating complexes consist of adaptor proteins that recruit and tether the minus end-directed microtubule motor protein cytoplasmic dynein (hereafter referred to as "dynein") to the cell cortex. Through the interaction of cortically

doi: https://doi.org/10.1534/genetics.117.300487
Manuscript received November 7, 2017; accepted for publication January 8, 2018; published Early Online January 18, 2018.
Supplemental material is available online at www.genetics.org/lookup/suppl/doi:10.1534/genetics.117.300487/-/DC1.
[1]Present address: Department of Molecular Biosciences, University of Texas at Austin, Austin, TX 78712.
[2]Corresponding author: Department of Biology, University of North Carolina at Chapel Hill, 616 Fordham Hall, Campus Box 3280, Chapel Hill, NC 27599-3280. E-mail: bobg@unc.edu

tethered dynein with the plus ends of astral microtubules, these complexes generate pulling forces that position the mitotic spindle within cells (Grill *et al.* 2003; Couwenbergs *et al.* 2007; Nguyen-Ngoc *et al.* 2007; Siller and Doe 2008; Williams *et al.* 2011). A conserved three protein complex—comprised of the membrane-anchored protein Gαi; the GoLoco and TPR repeat domain containing protein LGN; and NuMA, which is a microtubule and dynein-associated protein—often functions as the adapter that recruits dynein to the cell cortex (reviewed in Kotak and Gönczy 2013; Lu and Johnston 2013; see also Merdes *et al.* 1996; Gotta and Ahringer 2001; Couwenbergs *et al.* 2007; Park and Rose 2008; Yuzawa *et al.* 2011). In many known cases of oriented cell division, including in *Drosophila* neuroblast cells and multiple mammalian epithelial tissues, LGN is the first member of this complex that is positioned asymmetrically (Siller *et al.* 2006; Zheng *et al.* 2010; Peyre *et al.* 2011; Werts *et al.* 2011; Williams *et al.* 2011; Gloerich *et al.* 2017). NuMA can also be cortically enriched to achieve mitotic spindle orientation and, in some contexts, NuMA functions with partners other than LGN and Gαi, including Band 4.1 and Dishevelled (Ségalen *et al.* 2010; Kiyomitsu and Cheeseman 2012; Seldin *et al.* 2013). Mitotic spindles can also be oriented with symmetric localization of these complexes, including in the *Caenorhabditis elegans* zygote, where LIN-5/NuMA (Srinivasan *et al.* 2003) and DHC-1/Dynein (Schmidt *et al.* 2005) have been shown to be symmetrically localized during certain key phases of spindle positioning. In this case, LIN-5/NuMA activity has been shown to be asymmetrically regulated by phosphorylation (Galli *et al.* 2011).

Intercellular signaling has been shown to regulate mitotic spindle positioning through the enrichment of members of this complex to discrete domains of the cell cortex (Bergstralh *et al.* 2017). For example, in *Drosophila* sensory organ precursors, planar cell polarity pathway members Frizzled and Dishevelled recruit NuMA to one side of the precursor cell to orient the mitotic spindle along a specific axis (Ségalen *et al.* 2010). However, it is not clear whether members of this force-generating complex serve as a universal link between intercellular signaling pathways and the mitotic spindle, or whether there are alternative mechanisms by which intercellular signaling pathways can direct mitotic spindle positioning. In this work, we set out to better understand the mechanisms of mitotic spindle positioning directed by the Wnt signaling pathway, using as a model system the early *C. elegans* embryo.

The cell divisions in *C. elegans* embryos are highly stereotyped in both timing and orientation, and some cell divisions are known to be oriented by specific cell–cell interactions, making this an attractive system for investigating mechanisms of mitotic spindle positioning by cell–cell signaling (Goldstein 1995b; Schlesinger *et al.* 1999). At the four-cell stage, two neighboring cells—the germline precursor cell (P_2) and the endomesodermal precursor cell (EMS) (see Figure 1A)—use cell–cell signaling to orient their mitotic spindles toward their shared cell–cell contact. In the P_2 cell, signaling through the transmembrane receptor tyrosine kinase-like protein MES-1 serves as a spatial cue for the cortical enrichment of LGN (GPR-1 and GPR-2 in *C. elegans*) within P_2 at the contact with EMS (Werts *et al.* 2011). One pole of the P_2 spindle is pulled toward this domain of enriched GPR-1/2/LGN protein, positioning the spindle asymmetrically within the cell. However, in the neighboring EMS cell, GPR-1/2/LGN was found not to be enriched at the cell–cell contact, suggesting that a different mechanism of signaling-induced oriented cell division may be operating in EMS (Goldstein *et al.* 2006; Werts *et al.* 2011).

In EMS, contact with P_2, members of a highly conserved Wnt signaling pathway, and the MES-1 signaling pathway are required for both endodermal fate specification and for EMS mitotic spindle orientation (Goldstein 1992, 1993; Rocheleau *et al.* 1997; Thorpe *et al.* 1997; Schlesinger *et al.* 1999; Bei *et al.* 2002). Although β-catenin-dependent transcription of endodermal genes in the posterior daughter of EMS is required for endodermal cell fate, spindle positioning in EMS can occur without new transcription (Schlesinger *et al.* 1999). Two separate sets of experiments; one in *C. elegans* using isolated Wnt signaling cells and one in cultured mouse stem cells using purified, immobilized Wnt protein on beads; have demonstrated that Wnts can act as spatial cues to direct mitotic spindle positioning (Goldstein *et al.* 2006; Habib *et al.* 2013) (Figure 1B).

Many questions remain that are central to understanding Wnt-dependent spindle orientation. How does the Wnt signaling pathway provide positional information to drive rotation of the mitotic spindle into a specific axis? Does this response require enrichment of conserved spindle orientation pathway proteins such as NuMA and dynein, or are there other proteins involved? If proteins are enriched asymmetrically, how does that enrichment occur? In this work, we sought to address these questions and gain an increased mechanistic understanding of Wnt signaling-dependent mitotic spindle positioning.

Because of almost 20 years of interest in this and related questions, there is a sizable list of genes for which loss-of-function mutations, either alone or combined with disrupting the MES-1 and Src kinase signaling pathway, cause spindle orientation defects in the EMS cell (Schlesinger *et al.* 1999; Bei *et al.* 2002; Tsou *et al.* 2003; Walston *et al.* 2004; Zhang *et al.* 2008; Liro and Rose 2016). However, it is not known which of the identified genes might encode proteins that provide positional information to the mitotic spindle, and which have broader functions that are less directly relevant to this problem (for example, proteins that contribute more broadly to forming normal mitotic spindles). We view the current situation as akin to the old joke in which a scientist cuts off all of a frog's legs and claps loudly behind the frog. When the frog does not jump, the scientist concludes that frogs' ears are located on their legs. Many more components may be *required* for a response to a cue than just the sought-after parts needed to explain how a cue is initially received and transduced.

The challenge we sought to meet in this work was to identify proteins that might serve as positional cues downstream of

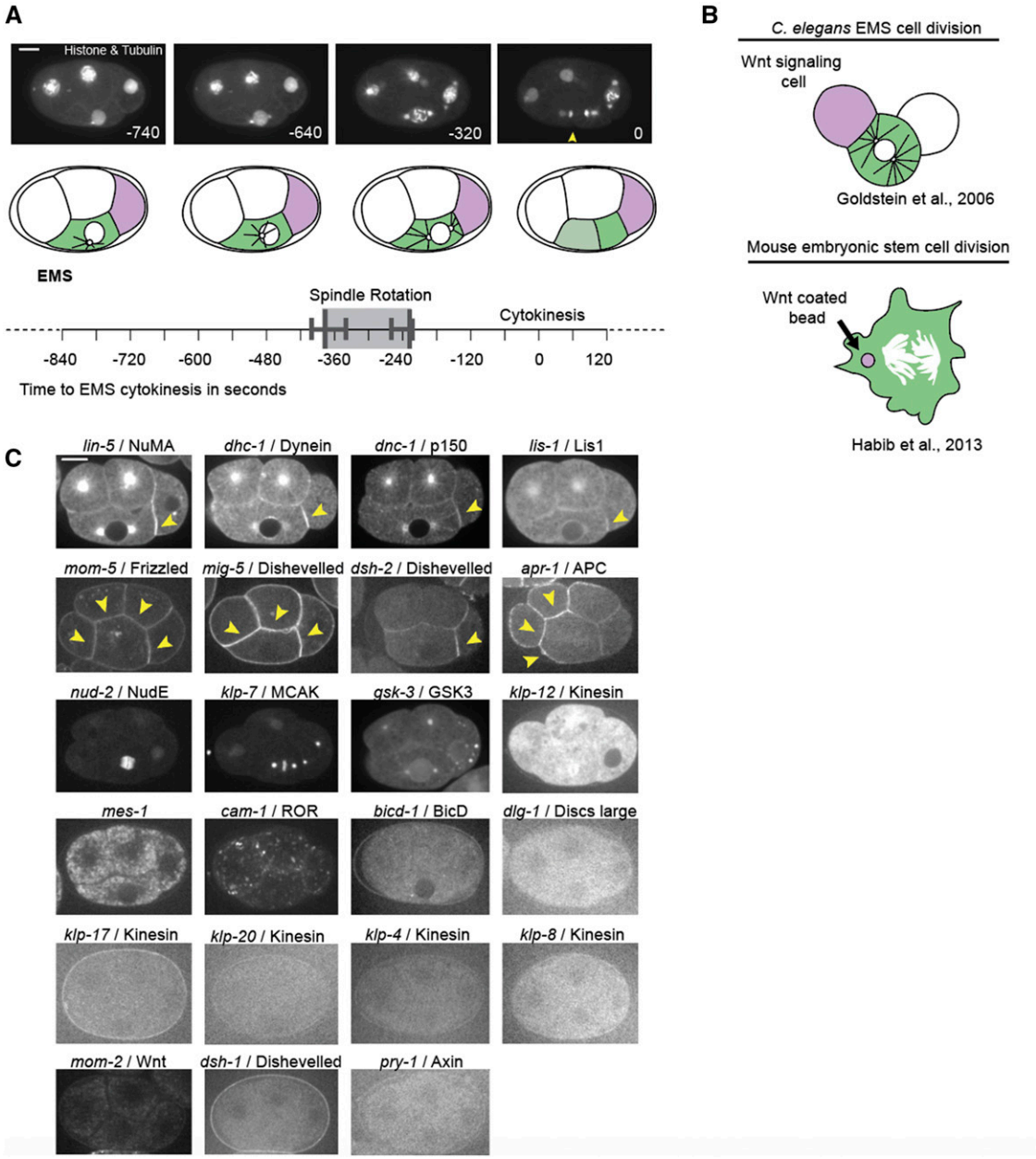

Figure 1 Localization of endogenously tagged candidate proteins. (A) Four-cell-stage *C. elegans* embryos labeled with GFP-histone and GFP-tubulin. Images are Z-projections through multiple imaging planes. Seconds before EMS cytokinesis are indicated in the bottom right of each image. Below the images are schematics of the four-cell-stage embryos with all cells labeled: the P_2, Wnt signaling cell, is colored purple and the responding EMS cell is colored in green; illustrating a lateral view of mitotic spindle rotation. The time line shows the period of mitotic spindle rotation as measured from three ventrally mounted embryos. The vertical lines at the ends of the gray box represent the average time of the beginning and end of rotation (373 and 233 sec prior to cytokinesis) and the bars encompass the range of measured values. Yellow arrowhead marks the site of cytokinesis in EMS. (B) A cartoon representation of two previously reported cases of Wnt-directed cell divisions. The source of Wnt (either a cell or a bead) is labeled in purple, and the responding cell whose division axis is oriented is green. (C) Four-cell-stage embryos from each strain generated. Each image is a single Z-slice through a center plane of an embryo, except for *cam-1*, which is a maximum projection. Yellow arrowheads mark cortical sites at which tagged proteins are enriched. Bars, 10 μm.

cell–cell signaling. Therefore, rather than seeking to define genes that are only required for spindle orientation, we took a different approach, seeking to use endogenously tagged protein localization *in vivo* to screen for key players. We sought to identify proteins that are (1) cortically localized, where they could respond to signaling inputs and contribute to force production on astral microtubules; (2) asymmetrically positioned along the ultimate axis of spindle positioning, the anterior–posterior axis of the embryo; and (3) asymmetrically localized in the EMS at the right time, during the period of spindle positioning. To accomplish this, we needed the ability to accurately visualize candidate proteins of interest over time while minimizing the likelihood of disrupting protein functions or generating overexpression artifacts. We also needed the

ability to make mosaic embryos, to determine which proteins were localized asymmetrically within EMS rather than only at the cortex of neighboring cells that contact EMS. Some tools such as antibodies and transgenic lines existed for certain candidate proteins (Supplemental Material, Table S1 in File S1), but they were not ideal for the purposes above. Therefore, we took the approach of inserting sequences encoding fluorescent protein fusion tags into the endogenous genetic loci of proteins of interest (Dickinson *et al.* 2013, 2015; Paix *et al.* 2014). We used these new strains to visualize the dynamic localizations of proteins of interest and to determine which are enriched at the EMS cortex specifically. Surprisingly, we found that members of the well-studied mitotic spindle positioning machinery LIN-5/NuMA and DHC-1/dynein were not detectably enriched asymmetrically in EMS. Instead, we found that two members of a Wnt pathway required for EMS spindle rotation, Dishevelled and adenomatous polyposis coli (APC) homologs, dynamically sort to the anterior and posterior cortex of EMS, respectively. These results identify specific proteins of future interest that could regulate spindle positioning either directly or through local regulation of force-generating complexes, and they highlight the utility of screening based on analyzing the localization of endogenously tagged proteins.

Materials and Methods

C. elegans strains

C. elegans animals were cultured on Normal Growth Media plates, fed *Escherichia coli* (OP50 strain), and grown at 20° for experiments. Worms were moved to 25° for incubation during strain construction. A list of strains generated for this work is available in Table S2 in File S1. Additional strains used are as followed: Bristol N2 (wild type), DP38 [*unc-119*(*ed3*) III], and XA3501 *ruIs32* [*pie-1*p::GFP::H2B + *unc-119*(+)] III. *ojIs1* [*pie-1*p::GFP::*tbb-2* + *unc-119*(+)].

Repair template construction and gene tagging

Strains were generated using methods from Dickinson *et al.* (2013, 2015) and Paix *et al.* (2014) (protocol used to create each strain is designated in Table S2 in File S1). The presence of multiple isoforms, the locations of catalytic or protein–protein interaction domains, as well as information about the functionality of previous tags were used to determine the fluorescent protein fusion site for a given protein (N or C terminus). Repair templates were constructed by inserting homology arm PCR products, amplified from worm genomic DNA, into vectors containing a fluorescent protein and a selection cassette via Gibson Assembly (New England Biolabs, Beverly, MA) as described in detail in Dickinson *et al.* (2013, 2015). Cas9 targeting sequences for each gene were selected using the CRISPR Design Tool (http://crispr.mit.edu). These sequences were cloned into the Cas9–single guide RNA expression vector DD162 (Dickinson *et al.* 2013), and co-injected into adult germlines with repair templates and array markers.

Candidate knock-ins were selected by drug treatment and phenotypic identification [roller (Rol)] as described in Dickinson *et al.* (2015) (except where indicated in Table S2 in File S1), and singled to new plates to establish independent lines. Candidate knock-ins with 100% Rol progeny were identified as putative homozygous insertions (C-terminal tags or nonessential genes); heterozygous insertions were isolated in the remaining cases (N-terminal tags of essential genes). To excise selectable elements, Cre was expressed in the candidate knock-ins, either by injection of a Cre-containing expression plasmid into the germline (Dickinson *et al.* 2013), or by heat-shock expression of Cre from the self-excising cassette (Dickinson *et al.* 2015). Candidate knock-ins were checked for expression of inserted tags using a dissecting microscope (Leica M165FC) equipped with a fluorescence light source (89 North PhotoFluor LM-75). In some cases, no fluorescence was detected using this method, presumably due to low gene expression levels. PCR genotyping was used to confirm homozygous insertion and removal of selectable makers in all isolated strains. In the cases of *klp-16* and *klp-18*, we observed significant embryonic lethality and those strains were not studied further. Embryonic lethality was quantified and negligible for the strains examined in Figure 2 and Figure 5 (Table S3A in File S1).

Genomic DNA isolation and genotyping

Genomic DNA was isolated from plates of worms using standard phenol–chloroform nucleic acid extraction and ethanol precipitation. Genomic DNA from candidate knock-in strains and N2 (unmodified) worms were used as templates for genotyping PCR reactions with LongAmp Taq DNA polymerase (New England Biolabs).

Microscopy

Embryos were dissected from gravid adults in Egg Buffer and mounted at the two- to four-cell stage on poly-L-lysine-coated coverslips with 2.5% agarose pads (as described in Marston *et al.* 2016). Cells isolated from embryos were mounted in Shelton's Medium using clay feet as spacers between the slide and coverslip. Both embryos and cells were imaged using a spinning disk confocal microscope with a Nikon (Garden City, NY) TiE stand and a 60× 1.4NA Plan Apo Oil Immersion Objective (Nikon), CSUXI spinning disk head (Yokogawa), and an ImagEM EMCCD (Hamamatsu). mNeonGreen (mNG) strains were excited using 514-nm solid state lasers with a 545/40 YFP emission filter set and were imaged in 690-MHz non-EM mode with varying exposure times. Single channel embryo and isolation samples were filmed at 20-sec intervals. To prepare figures, images were cropped and rotated, and brightness and contrast were adjusted using Fiji.

RNA interference

Adult animals were injected with double-stranded RNAs (dsRNAs) targeting specific gene products according to standard procedures (Dudley *et al.* 2002). The concentrations of dsRNAs injected are available in Table S3C in File S1.

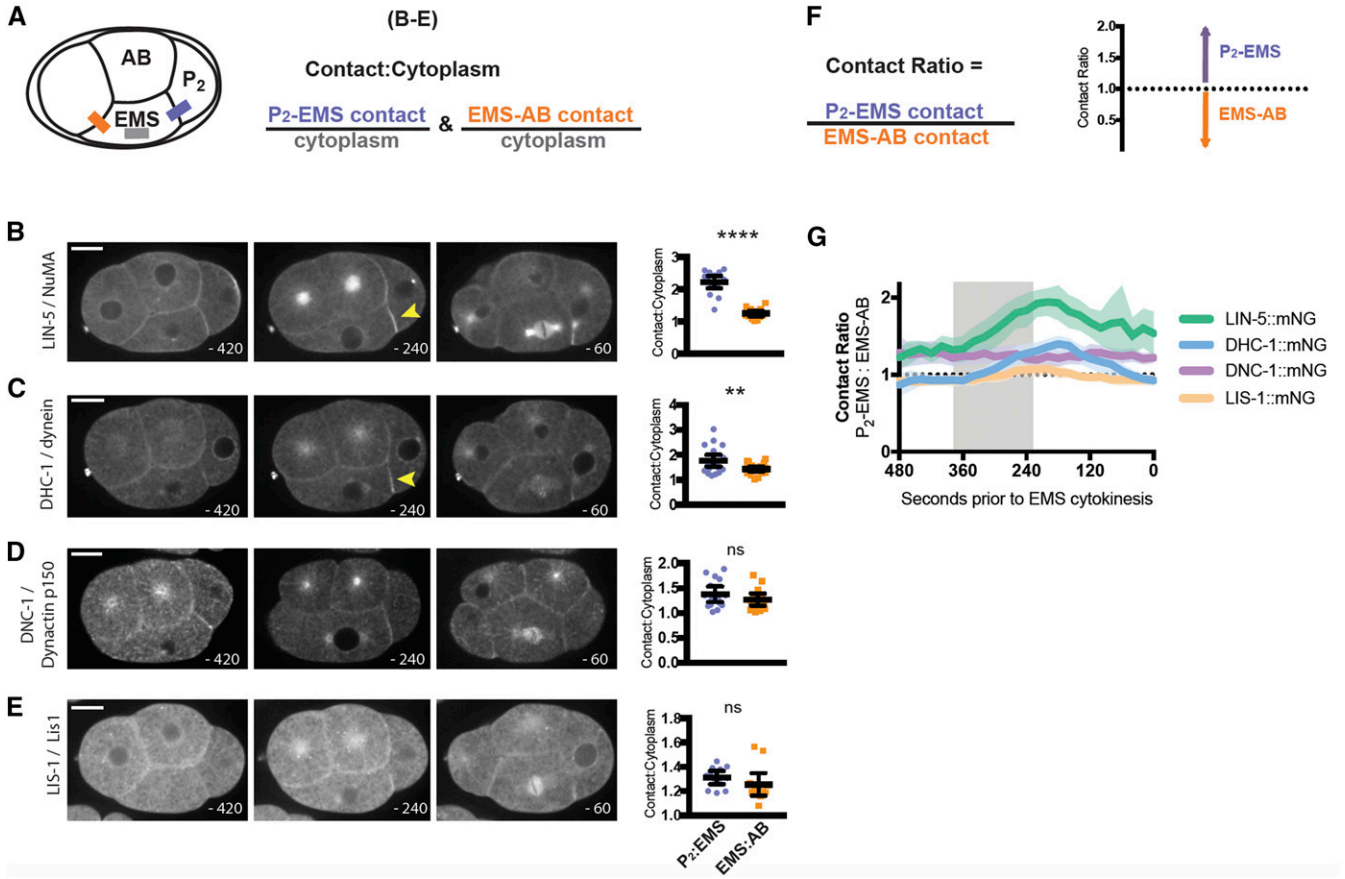

Figure 2 Localization of LIN-5/NuMA, DHC-1/dynein, DNC-1/dynactin p150, and LIS-1/Lis1 during the EMS cell cycle. (A) Schematic describing the strategy for quantification of fluorescence at the cell–cell contacts during spindle rotation (P_2–EMS contact is purple, EMS–AB contact is orange, cytoplasm is gray). (B–E) Localization of tagged proteins at three different times during the EMS cell cycle. Images are single Z-planes. Quantification was performed during spindle rotation at 260 sec prior to EMS division. Seconds before EMS division are indicated at the bottom right of each panel. NuMA: $n = 16$, **** $P < 0.0001$; Dynein Heavy Chain: $n = 21$, ** $P = 0.0096$; Dynactin p150: $n = 16$, $P = 0.25$ (NS); Lis1: $n = 12$, $P = 0.26$ (NS). Statistical test used was an unpaired *t*-test. Black lines represent means and 95% confidence intervals. Gray bar is the period during which the EMS spindle rotates. Yellow arrowheads mark cortical site at which tagged proteins are enriched. (F) Schematic describing the strategy for quantification of fluorescence at the cell–cell contacts over time, expressed as a ratio of the fluorescence intensity at the P_2–EMS contact and EMS–AB contact. (G) Ratios of intensity at the P_2–EMS contact and EMS–AB contact over time for each strain in (B–E). Colored lines represent means, and lighter colors are 95% confidence intervals. Bars, 10 μm.

Embryos were dissected from injected adults and imaged 18–28 hr postinjection. At least three samples per experiment were prepared by mounting control embryos (from uninjected worms) side by side with RNA interference (RNAi)-treated embryos for direct comparison and quantification. Additional samples were mounted in groups of treated or untreated embryos and imaged under identical conditions as the paired embryos.

Cell isolations

Cells were isolated from embryos and cultured as described previously (Edgar and Goldstein 2012). Chitinase from *Streptomyces griseus* was used at a concentration of 20 unit/ml dissolved in Egg Buffer to remove eggshells (C6137; Sigma Chemical, St. Louis, MO). To isolate P_2–EMS cell pairs, eggshells were removed at the two-cell stage, the P_1 and AB cells were separated, and the division timing of the P_1 cell was tracked. Recombinations of P_2–EMS cell pairs, or individual EMS, were performed within 4 min after EMS birth (Goldstein 1995a). Cells were cultured in Shelton's Medium and mounted on glass slides with coverslips for imaging (Werts *et al.* 2011).

Quantification and statistical analysis

A 5-pixel-wide line was drawn through each contact of interest, the cytoplasm, and off-embryo background in Metamorph (Molecular Devices). A kymograph was generated using the 5-pixel average. From that kymograph, the maximum pixel intensity for each contact was recorded and the average pixel intensity of the cytoplasm and off-embryo background was recorded for each time point. Fluorescence intensity was calculated by subtracting off-embryo background from the pixel intensity values for the contact and cytoplasm. Fluorescence intensities measured at the contacts were normalized by dividing by average fluorescence intensity of the cytoplasm. Fiji and Metamorph software (Molecular Devices) were used to quantify fluorescence intensity from micrographs. Mean intensity values were compared at 260 sec prior to EMS

cytokinesis, a time point near the end of spindle rotation (Figure 1A) when we predicted cortical asymmetries might be maximal. Unpaired *t*-tests with Welch's correction were used to compare means and were performed using GraphPad Prism 7 software. *P*-values and *n* values for each experiment are reported in figures, figure legends, or text.

Data availability

Strains generated for this work will be made available through the *Caenorhabditis Genetics Center*. Plasmids are available upon request. The authors affirm that all data necessary for confirming the conclusions of the article are present within the article, figures, and tables.

Results

Endogenous tags reveal localization and dynamics of candidate proteins at the four-cell stage

To identify proteins that might act as positional cues for mitotic spindle orientation in EMS, we first generated a list of 26 candidate proteins that included microtubule-associated motor proteins, motor protein regulators, signaling pathway members, and proteins required for normal spindle rotation in EMS (for convenience, we use the term "spindle rotation" here to refer to rotation of a spindle during mitosis or the earlier rotation of a centrosomes–nucleus complex, orienting the future spindle). We took advantage of CRISPR-Cas9-triggered homologous recombination strategies to insert genes encoding fluorescent proteins at the endogenous loci encoding the candidate proteins (Dickinson *et al.* 2013, 2015; Paix *et al.* 2014).

Tools such as antibodies and transgenes existed previously for some of our proteins of interest, including some antibodies (nine) and rescuing transgenes (three) (Table S1 in File S1) (Skop and White 1998; Gönczy *et al.* 1999; Berkowitz and Strome 2000; Bossinger *et al.* 2001; Firestein and Rongo 2001; McMahon *et al.* 2001; Oegema *et al.* 2001; Bei *et al.* 2002; Hawkins *et al.* 2003, 2005; Srinivasan *et al.* 2003; Cockell *et al.* 2004; Park *et al.* 2004; Walston *et al.* 2004; Schmidt *et al.* 2005; Gassmann *et al.* 2008; Zhang *et al.* 2008; Song *et al.* 2010; Sugioka *et al.* 2011; Chien *et al.* 2015; Han *et al.* 2015; Barbosa *et al.* 2017). However, we chose to insert tags into endogenous loci for three reasons. First, they allowed us to visualize protein localization and dynamics via live imaging throughout the cell cycle, and to directly compare protein dynamics in embryos under different treatment regimes. Second, endogenously tagged proteins are generally expected to be expressed at normal levels, using their native promoters and regulatory elements, and 100% of the native protein is labeled (Dickinson *et al.* 2013; Kim *et al.* 2014). This is critical as previous studies have revealed that overexpression of proteins involved in spindle orientation and signaling pathways can result in aberrant phenotypes (Werts *et al.* 2011). Third, although antibodies would similarly report the localization of candidate proteins with accuracy, due to the resolution limits of confocal microscopy, when a protein is enriched at a cell–cell contact, immunofluorescence is not sufficient to determine which cell contains the candidate protein. Endogenous tags permit experiments to test whether P_2–EMS boundary localization is explained by enrichment at the boundary in one cell, the other, or both by making mosaic embryos through direct cell manipulation (Werts *et al.* 2011).

We successfully isolated homozygous fluorescent protein knock-in strains for 23 of the 26 candidate genes (See *Materials and Methods*, Figure 1, and Table S2 in File S1). For the three remaining genes, we observed significant embryonic lethality in the progeny of *klp-16* and *klp-18* candidate knock-ins, precluding analysis because of presumed effects of the addition of the fluorescent protein tag to the gene product. We failed to isolate candidate knock-ins for *klp-3* for unknown reasons.

Among the 23 genes tagged, we identified 14 genes with detectable early embryonic protein products (Figure 1C and Figure S1 in File S1), 12 of which had clear localization patterns at the four-cell stage (Figure 1C, top three rows). Cortical pulling forces often dominate mitotic spindle positioning (Grill and Hyman 2005), and eight of the protein products we observed appeared enriched at cell cortices at the four-cell stage (Figure 1C, top two rows). One of these proteins was cytoplasmic dynein (DHC-1/Dynein heavy chain) and three were dynein-associated proteins: DNC-1/Dynactin p150, LIS-1/Lis1, and LIN-5/NuMA (Figure 1C, top row). The other four proteins were members of a Wnt signaling pathway known to regulate the EMS mitotic spindle (Figure 1C, second row) (Schlesinger *et al.* 1999; Bei *et al.* 2002; Sugioka *et al.* 2011). The overall localization patterns of our endogenous tags matched previously reported localization patterns based on antibody staining and nonendogenously tagged transgenes (Skop and White 1998; Gönczy *et al.* 1999; Berkowitz and Strome 2000; Bossinger *et al.* 2001; Firestein and Rongo 2001; McMahon *et al.* 2001; Oegema *et al.* 2001; Bei *et al.* 2002; Hawkins *et al.* 2003, 2005; Srinivasan *et al.* 2003; Cockell *et al.* 2004; Park *et al.* 2004; Walston *et al.* 2004; Schmidt *et al.* 2005; Gassmann *et al.* 2008; Zhang *et al.* 2008; Song *et al.* 2010; Sugioka *et al.* 2011; Chien *et al.* 2015; Han *et al.* 2015; Barbosa *et al.* 2017). We did not observe gain- or loss-of-function phenotypes in our imaging experiments and measured no significant embryonic lethality (Table S3A in File S1). Because many of the proteins we tagged are essential proteins, we infer from the lack of embryo lethality that the tags on these proteins did not disrupt essential functions.

We next examined the fusion proteins that were undetectable or nearly undetectable at the four-cell stage (Figure 1A, bottom three rows). In every case, we could detect fluorescence at later stages of embryogenesis, in larvae, and/or in adult animals (Figure S1 and Table S4 in File S1); suggesting that these genes are either not expressed early in development, or are too transient or at such low levels as to be below our threshold of detection. Many of the expression patterns at later stages were consistent with known roles of these proteins; for example, CAM-1, a Ror receptor tyrosine kinase homolog, localized to the plasma membrane (Figure S1 in

File S1) (Green *et al.* 2007). Interestingly, although loss of KLP-17 has been shown to cause embryonic lethality at the one- and two-cell stage, we detected the KLP-17::mNG in the sperm (Figure S1 in File S1, top row, far right) (Ali and Siddiqui 2000). These results confirm that the fusion proteins we failed to detect at the four-cell stage were indeed successfully tagged, and suggest that our inability to detect them in early embryos is due to low (or absent) embryonic expression.

One important outcome of our screening approach is the resulting collection of tagged strains, which will be made available to other laboratories. Because each tagged gene is controlled by its endogenous regulatory elements, in its native context in the genome, it is likely to be expressed at each stage at which the endogenous gene functions. These strains can be used to study the dynamic properties of these 23 proteins at various developmental stages.

Live imaging of LIN-5 and DHC-1 reveals the dynamics of enrichment at the P_2–EMS contact

To begin to understand when and in which cells proteins become localized, we imaged our mNG-tagged fusion proteins throughout the EMS cell cycle using spinning disk confocal microscopy (Figure 2). Proteins that function as positional cues for mitotic spindle positioning often occupy a specific domain of the cell cortex toward which spindle poles are pulled (Lechler and Fuchs 2005; Siller *et al.* 2006; Zheng *et al.* 2010; Peyre *et al.* 2011; Werts *et al.* 2011; Williams *et al.* 2011; Gloerich *et al.* 2017). Because we knew that P_2 functions as a positional cue for EMS mitotic spindle positioning (Goldstein 1995b), we predicted that force-generating complexes might be enriched in EMS where it contacts P_2. Therefore, to test whether our tagged proteins were enriched at the P_2–EMS contact, we compared the normalized mean fluorescence intensity at the P_2–EMS contact to the mean intensity at an EMS-AB (for convenience, we use "AB" here to refer to ABa or ABp) cell contact during spindle rotation in EMS (Figure 2, B–E; −260 sec prior to EMS cytokinesis).

We first examined the localization of LIN-5/NuMA using LIN-5::mNG. Previous experiments using a temperature-sensitive allele of *lin-5* demonstrated that *lin-5*/NuMA function is required for proper spindle positioning in EMS (Liro and Rose 2016). Consistent with previous antibody staining for LIN-5/NuMA, LIN-5::mNG was localized at cell contacts and centrosomes and it decorated spindle microtubules in metaphase and anaphase (Figure 2B) (Lorson *et al.* 2000). LIN-5::mNG was enriched at the P_2–EMS contact relative to an EMS–AB contact during EMS spindle rotation (Figure 2B). This enrichment peaked after rotation was complete (Figure 2G).

We next examined *in vivo* localization of cytoplasmic dynein heavy chain, DHC-1. Regulators of dynein, including the dynactin subunit *dnc-1*/p150^{glued}, have been shown to be required for EMS spindle rotation (Zhang *et al.* 2008). We observed that DHC-1::mNG was diffuse in the cytoplasm, decorated structures likely to be microtubules and centrosomes, and was strongly enriched at the nuclear envelope and at kinetochores during metaphase (Figure 2C). These results are consistent with previous observations of DHC-1 immunohistochemistry, using transgenic fluorescent protein fusions in which function of tagged protein had not been assessed, and a recently reported CRISPR knock-in allele (Gönczy *et al.* 1999; Malone *et al.* 2003; Schmidt *et al.* 2005; Gassmann *et al.* 2008; Barbosa *et al.* 2017). DHC-1::mNG was also enriched at the P_2–EMS contact during EMS spindle rotation (Figure 2C). Similar to LIN-5::mNG, this enrichment continued throughout EMS spindle rotation and peaked almost a minute after rotation was complete. Two tagged regulators of dynein, DNC-1::mNG and LIS-1::mNG, also had some cortical localization at the four-cell stage, consistent with previous reports (Cockell *et al.* 2004; Zhang *et al.* 2008). However, we did not detect a significant difference in fluorescence intensity at the P_2–EMS contact *vs.* the EMS–AB cell contact for either DNC-1::mNG or LIS-1::mNG (Figure 2, D and E). Taken together, these results are consistent with previous suggestions (Werts *et al.* 2011) that accumulation of LIN-5, dynein regulators, or both, at the EMS cortex could contribute to signaling-induced mitotic spindle positioning.

LIN-5/NuMA is enriched in P_2 and not asymmetric in EMS during spindle rotation

It was previously shown via immunostaining that LIN-5/NuMA enrichment at the P_2–EMS contact was not affected by loss of the Wnt receptor *mom-5*/Frizzled, but was reduced in *mes-1* mutants (Srinivasan *et al.* 2003). To confirm that LIN-5/NuMA enrichment at the P_2–EMS contact was Wnt independent, we targeted the Wnt ligand *mom-2* by dsRNA injection. This treatment caused observable spindle orientation defects in EMS in some embryos and caused lethality in all examined embryos (10/10), consistent with maternal phenotypes observed in the embryos of *mom-2* mutant worms (Thorpe *et al.* 1997) and with the expectation that RNAi reduced the activity of the Wnt pathway as expected. However, *mom-2* RNAi did not reduce the level of LIN-5::mNG enrichment at the P_2–EMS contact (Figure 3A). We also confirmed that targeting *mes-1* similarly significantly reduced LIN-5::mNG accumulation at the P_2–EMS contact (Figure 3B).

Although these data show that LIN-5::mNG is enriched at the P_2–EMS contact, diffraction-limited light microscopy cannot resolve whether the protein enrichment occurs within P_2, EMS, or both. One possible source of LIN-5:mNG enrichment at the P_2–EMS contact is that enrichment occurs within P_2. The LIN-5/NuMA binding partner GPR-1/2/LGN was previously shown to be enriched at this cell–cell contact within P_2 but not EMS, raising the possibility that LIN-5/NuMA follows the same pattern (Werts *et al.* 2011). A second possibility is that LIN-5::mNG is enriched within EMS. In this case, we might predict that Dishevelled acts as the cortical adapter for LIN-5/NuMA, as is the case in *Drosophila* sensory organ precursors (Ségalen *et al.* 2010). To distinguish between these possibilities, we tested whether LIN-5/NuMA is enriched in P_2, EMS, or both cells, by constructing mosaic embryos by hand, placing LIN-5::mNG P_2:EMS cell pairs

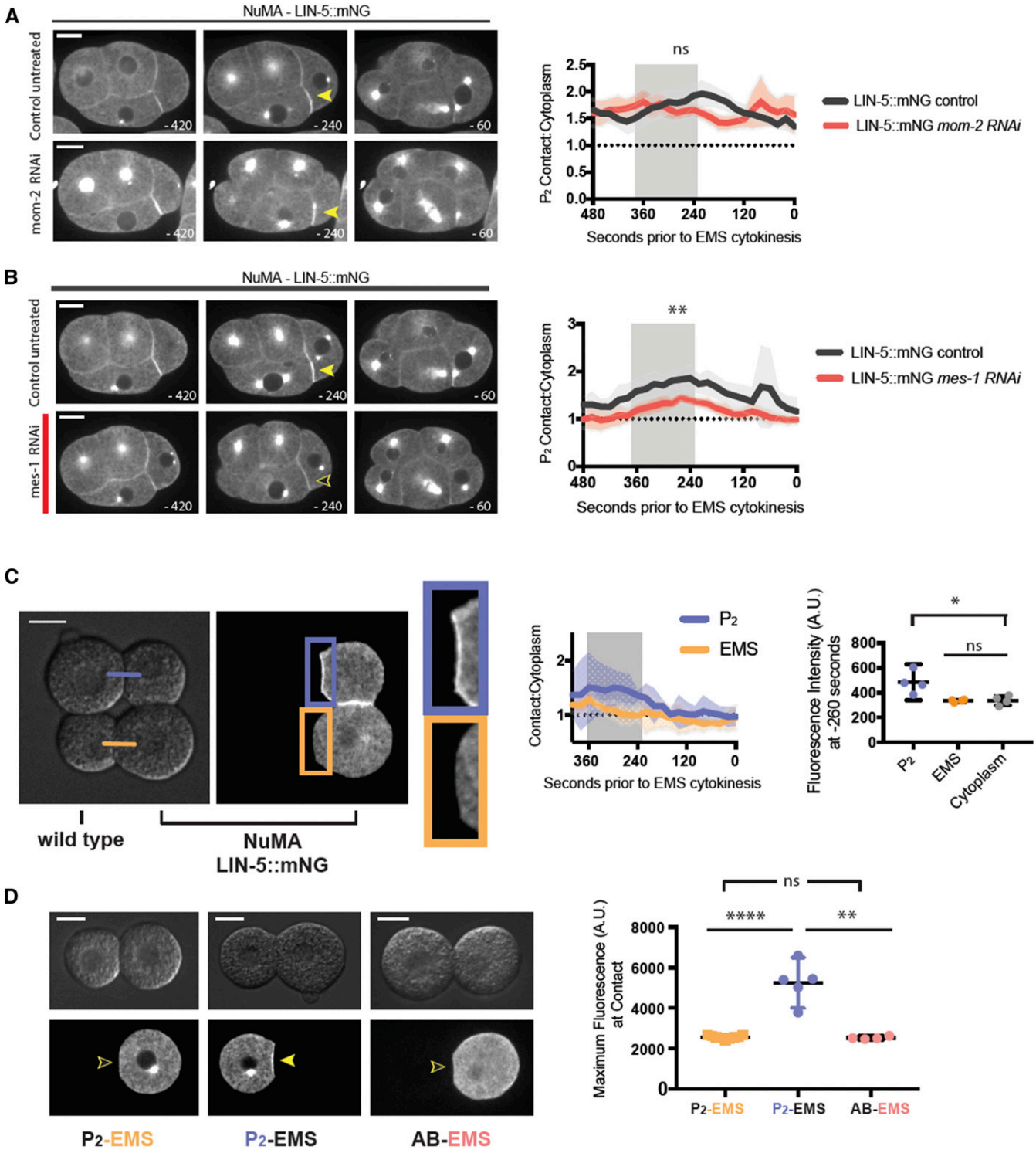

Figure 3 LIN-5/NuMA is enriched in P_2 at the contact with EMS. (A) Live imaging of embryos expressing LIN-5::mNG in control and *mom-2* RNAi conditions. Arrowheads point to enrichment of LIN-5::mNG at P_2–EMS contact site. Control: $n = 17$; *mom-2* RNAi: $n = 20$. Statistical test performed during spindle rotation (−260 sec), $P = 0.15$ (NS). (B) Embryos expressing LIN-5::mNG in control and *mes-1* RNAi conditions. Control: $n = 7$; *mes-1* RNAi: $n = 7$. Statistical test performed during spindle rotation (−260 sec), ** $P = 0.0014$. (C) Partial embryos made by direct manipulation of unlabeled and LIN-5::mNG-labeled P_2 and EMS pairs. P_2 are the smaller cells. Purple and orange lines represent new contacts where fluorescent protein levels were quantified, $n = 4$. Plot compares fluorescence intensity at the contacts to the cytoplasmic fluorescence intensity. P_2 contact *vs.* cytoplasm, * $P = 0.025$; EMS contact *vs.* cytoplasm, $P = 0.87$ (NS). (D) Recombined LIN-5::mNG and unlabeled cells. Arrowheads point to cell contacts. Plot is the maximum fluorescence reached during the EMS cell cycle. P_2–EMS, $n = 9$; P_2–EMS, $n = 5$; AB–EMS, $n = 4$. Solid lines indicate means with 95% confidence intervals. $P = 0.59$ (NS), ** $P = 0.0011$, **** $P < 0.0001$. Bars, 10 μm.

and unlabeled P_2–EMS cell pairs in contact to create two new P_2:EMS contact sites (Figure 3C). This arrangement allows both P_2 and EMS enrichments to be compared in single experiments. We measured the fluorescence intensity at the contacts between labeled and unlabeled cells during EMS spindle rotation, and we found an enrichment of protein at the P_2–EMS contact in P_2, but not in EMS (Figure 3C).

To rule out the possibility that an additional signaling cell contact in the experiment above might obscure detection of protein enrichment in EMS, we recombined labeled and unlabeled single cells and measured the maximum fluorescence intensity at the contacts. The results confirmed that there is a significant accumulation of LIN-5::mNG at the P_2–EMS contact in P_2, but not in EMS (Figure 3D). To determine whether the low level of LIN-5::mNG enrichment in EMS near P_2 is detectably any greater than that expected from EMS contact with a nonsignaling cell, we placed a labeled LIN-5::mNG EMS in contact with a non-Wnt signaling, unlabeled AB cell (Figure 3D). We did not see a significant difference in the amount of LIN-5::mNG at the EMS cortex, whether EMS was in contact with a Wnt-signaling P_2, or a nonsignaling AB cell (Figure 3D). These results suggest that LIN-5::mNG is enriched at the cell cortex within P_2 but not in EMS. We conclude that LIN-5/NuMA is unlikely to act as an asymmetrically localized cue for mitotic spindle positioning in EMS.

DHC-1/dynein is not enriched asymmetrically in EMS

The dynein regulators we have examined to this point are not asymmetrically localized in EMS (Figure 2 and Figure 3). However, it is possible that other unknown cortical adapters tether dynein at the P_2–EMS contact in response to Wnt signaling. Therefore, we next tested whether the enrichment of DHC-1::mNG we observed at the P_2–EMS contact (Figure 2C) was Wnt dependent. Targeting the Wnt ligand *mom-2* by RNAi resulted in some DHC-1::mNG embryos exhibiting spindle rotation defects and all treated embryos failing to develop (12/12), but only a slight change in the timing of enrichment, and no change in the maximum enrichment of DHC-1::mNG at the P_2–EMS contact (Figure 4A); suggesting that Wnt signaling might not be necessary for DHC-1/dynein enrichment at the P_2–EMS contact. This result suggested to us that the enrichment of DHC-1::mNG at the P_2–EMS contact might not reflect enrichment within the EMS cell. To test this directly, we recombined unlabeled P_2 cells with DHC-1::mNG-expressing EMS (Figure 4B). We detected no enrichment of DHC-1::mNG at the P_2–EMS contact relative to a noncell-contacting region of the EMS cortex (Figure 4B). Because DHC-1::mNG is not enriched asymmetrically within EMS to the site of contact, we conclude that DHC-1/dynein is unlikely to act as an asymmetrically localized cue for spindle positioning in EMS at its site of contact with P_2.

Taken together, our results for LIN-5::mNG and DHC-1::mNG suggest that although members of the Gα/LGN/NuMA and dynein complex are genetically required for spindle rotation in EMS, they are not enriched in the posterior EMS cortex during spindle rotation (Figure 3 and Figure 4) (Tsou *et al.* 2003; Zhang *et al.* 2008; Liro and Rose 2016). We conclude that the signals that direct EMS spindle positioning do not locally enrich DHC-1/dynein-containing complexes to a specific site in the EMS cortex, unlike in other cases of oriented cell division (Woodard *et al.* 2010; Kiyomitsu and Cheeseman 2012, 2013; Tame *et al.* 2014). GPR-1/2/LGN (Werts *et al.* 2011) and LIN-5/NuMA are instead asymmetrically enriched at the cortex of P_2 and are likely function to locally tether DHC-1/dynein to achieve spindle positioning in P_2.

Localization of endogenously tagged Wnt pathway components reveals timing of EMS polarization

In our initial screen, we identified four additional fusion proteins as having some cortical localization at the four-cell stage: MOM-5::YPET, mNG::DSH-2, mNG::MIG-5, and mNG::APR-1 (Frizzled, Dishevelled, and APC homologs, respectively) (Figure 1A). Previous studies have demonstrated that *mom-5*/Frizzled, *dsh-2*/Dishevelled, and *mig-5*/Dishevelled loss of function or depletion results in defects in EMS spindle positioning and that APR-1/APC contributes to astral microtubule asymmetry after spindle orientation, stabilizing microtubules in the anterior of EMS during telophase (Walston *et al.* 2004; Sugioka *et al.* 2011). To determine whether these proteins might be acting as asymmetrically localized cues for EMS spindle positioning, we examined the dynamics of their localization during the EMS cell cycle (Figure 5).

To our knowledge, the localization of the Wnt receptor MOM-5/Frizzled was previously unknown at the *C. elegans* four-cell stage. We found MOM-5::YPET to be distributed at the plasma membrane of all four cells, and most enriched at cell–cell contacts (Figure 5A). Additionally, MOM-5::YPET labeled a pool of dynamically moving internal cell membranes, including the internalizing midbody remnant in the anterior of EMS (Figure 5A, arrow) (Singh and Pohl 2014). We did not detect statistically significant enrichment of MOM-5::YPET at the P_2–EMS contact over EMS–AB cell contacts during spindle rotation (Figure 5A). The lack of MOM-5/Frizzled polarity at the four-cell stage contrasts with the polarized domains of Frizzled found in later stage asymmetric divisions of AB lineage blastomeres (Park *et al.* 2004) and the postembryonic T cell (Goldstein *et al.* 2006) (MOM-5/Frizzled and LIN-17/Frizzled, respectively).

Dishevelled is a component of the Wnt signaling pathway that binds the intracellular domain of Frizzled when Frizzled is activated by a Wnt ligand (Wong *et al.* 2003). It was previously reported, using antibody staining, that DSH-2/Dishevelled is enriched at the P_2–EMS contact, and that this cortical localization is dependent on *mom-5/Frizzled* (Walston *et al.* 2004; Hawkins *et al.* 2005). Our observations of mNG::DSH-2 are consistent with the previously reported cortical localization and enrichment at the P_2–EMS contact (Figure 5B), which we quantified over time (Figure 5E). We did not see a significant difference in fluorescence intensity between the P_2–EMS and EMS–AB contacts during mitotic

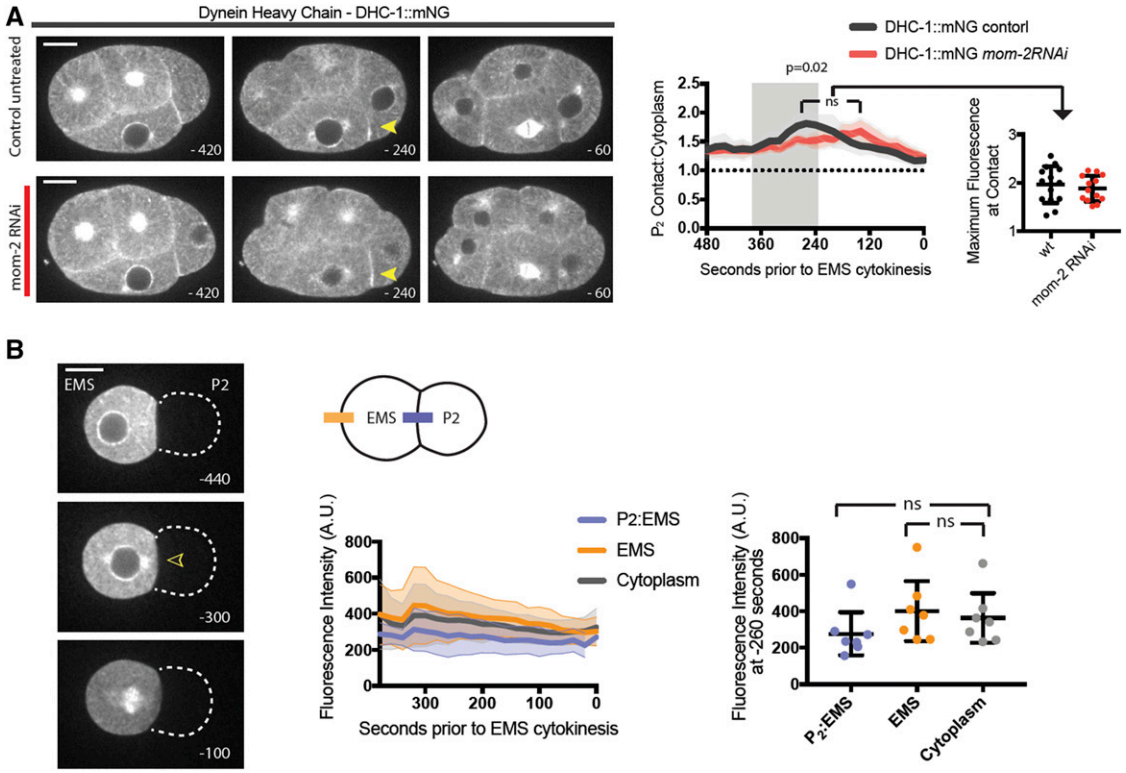

Figure 4 DHC-1/Dynein is not enriched in EMS at the P_2–EMS contact. (A) Live imaging of embryos expressing DHC-1::mNG in control and *mom-2* RNAi conditions. Arrowheads point to enrichment of DHC-1::mNG at P_2–EMS contact site. Control, n =13; *mom-2* RNAi, n =12. In graph at right: colored lines represent means, and lighter colors are 95% confidence intervals. Statistical test performed during spindle rotation (−260 sec), P = 0.02. The maximum intensity at the P_2–EMS contact compared in control *vs. mom-2* RNAi, P = 0.53 (NS). (B) Recombined DHC-1::mNG and unlabeled cells. Arrowheads point to cell contacts. n = 10. P_2–EMS *vs.* cytoplasm, P = 0.26 (NS); EMS cortex *vs.* cytoplasm, P = 0.67 (NS). Diagram depicts positions of line scans used for quantification. Bar, 10 μm.

spindle rotation. However, the level of mNG::DSH-2 continued to rise after spindle rotation and peaked ~120 sec before EMS cytokinesis (Figure 5E). Another tagged Dishevelled homolog, mNG::MIG-5, had a pronounced localization to all cell contacts (Figure 5C), and was slightly enriched at the P_2–EMS boundary compared to the EMS–AB boundary during EMS spindle rotation (Figure 5C). Taken together, these results suggest that the two major Dishevelleds implicated in spindle rotation in EMS are enriched at the P_2–EMS contact. Combining an unlabeled P_2 cell and an mNG::DSH-2-labeled EMS revealed that, as expected, DSH-2 is enriched in EMS at the P_2–EMS contact (Figure 5F).

APC is a key component of the β-catenin destruction complex. The *C. elegans* APC homolog APR-1 regulates mitotic spindle asymmetry and microtubule stability in EMS during telophase and a GFP::APR-1 transgene, whose function after tagging was not tested, was previously shown to become enriched in the anterior cortex of EMS, gradually during mitosis (Sugioka *et al.* 2011). APR-1 was also shown to affect the distribution of fate determinants in the EMS daughter cells (Sugioka *et al.* 2011). We examined mNG::APR-1 localization throughout the EMS cell cycle and found that mNG::APR-1 is enriched in the anterior of EMS and largely excluded from the P_2–EMS contact (Figure 5D). This asymmetry is apparent early (before 480 sec prior to EMS division), which is earlier than any other molecular asymmetry we have observed so far. The localization we observed for functionally tagged APC/APR-1 is similar to the asymmetry reported previously using a transgene (Sugioka *et al.* 2011). However, we observed that the asymmetry begins earlier in the cell cycle: prior to and during spindle rotation. This asymmetry of mNG::APR-1 across EMS was visible in cortical planes, where distinct and relatively stable puncta of mNG::APR-1 could be seen, ranging in stability from appearing in just one frame (taken at 1-sec intervals) to a maximum of 11.6 ± 1.2 sec (95% C.I.; most stable 20 puncta per embryo, n = 13 embryos) (Figure S2 in File S1). We observed that the cortical mNG::APR-1 became asymmetric in the ABp cell as well, mirroring the distribution and timing of APR-1/APC localization in EMS (Figure S2 in File S1). These observations and further experiments below establish that both Dishevelled and APC are asymmetrically localized on opposite sides within EMS during the period of spindle positioning.

mom-2/Wnt is a necessary spatial cue for polarization of APR-1 and DSH-2

We noticed that in the latter half of the EMS cell cycle, Dishevelled and APC appear to be occupying distinct cortical domains in the EMS cortex, consistent with previous reports using antibodies and transgenes during a narrower part of the

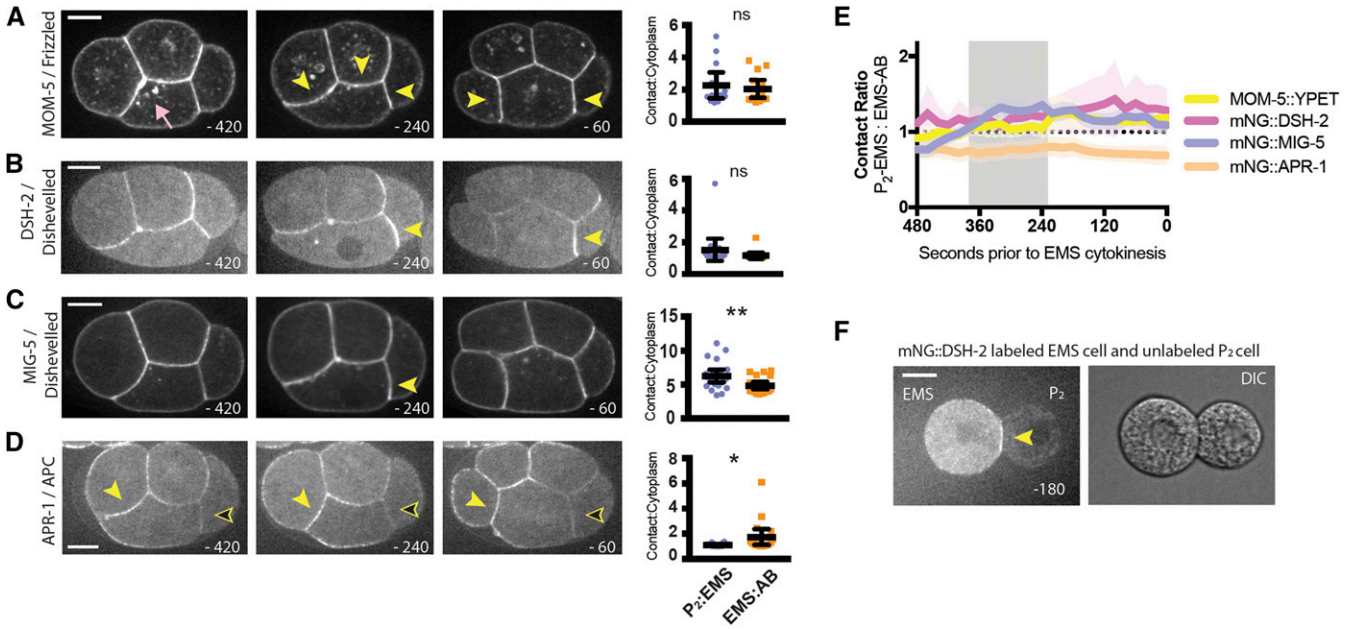

Figure 5 Localization of MOM-5/Frizzled, DSH-2/Dishevelled, MIG-5/Dishevelled, and APR-1/APC during the EMS cell cycle. (A–D) Localization of tagged proteins at three different times during the EMS cell cycle. Images are single Z-planes. Quantification was performed during spindle rotation at 260 sec prior to EMS division. Time is indicated in seconds before EMS division at the bottom right of each panel. MOM-5: $n = 13$, $P = 0.64$ (NS); DSH-2: $n = 15$, $P = 0.28$ (NS); MIG-5: $n = 22$, ** $P = 0.0089$; APC $n = 18$, * $P = 0.04$. Black lines represent means and 95% confidence intervals. Gray bar is the period during which the EMS spindle rotates. Yellow arrowheads mark cortical sites at which tagged proteins are enriched. Arrowheads filled with black mark a cortical site at which tagged proteins are not enriched. (E) Ratio of intensity at the P_2–EMS contact and EMS–AB contact over time for each strain shown in (A–D). Colored lines represent means and lighter colors are 95% confidence intervals. (F) Recombined cell pair of unlabeled P_2 and mNG::DSH-2-labeled EMS at 180 sec prior to EMS cytokinesis, $n = 3$. Bars, 10 μm.

cell cycle (Walston *et al.* 2004; Sugioka *et al.* 2011). Because these proteins are downstream members of the Wnt pathway, we hypothesized that Wnt signaling would be important for these polarized localization patterns. To test this hypothesis, we injected dsRNA targeting the Wnt ligand *mom-2*. We found that mNG::DSH-2 failed to become enriched at the P_2–EMS contact in *mom-2* RNAi-treated embryos (Figure 6A). When we compared control and *mom-2* RNAi-treated embryos for mNG::APR-1, we observed that mNG::APR-1 was no longer restricted to the anterior of EMS (Figure 6B). The mNG::APR-1 cortical domain expanded to the P_2–EMS contact in some embryos, enriching strongly over cytoplasmic levels, although this was not seen in all embryos (Figure 6B). Taken together with the finding that Wnt and Frizzled affect DSH-2 localization (Figure 6B) (Hawkins *et al.* 2005), this result suggests that Wnt-dependent recruitment of Dishevelled at the P_2–EMS contact might contribute to excluding APC from the posterior cortex of EMS, which we further test below.

To investigate the dynamics of these proteins simultaneously in the same embryos, we generated a dual-labeled strain with both mNG::DSH-2 and mScarlet::APR-1. We observed that mScarlet::APR-1 enriched in the anterior of EMS and mNG::DSH-2 enrichment in the posterior (Figure 6C). To observe polarization specifically within EMS, we recombined unlabeled P_2 signaling cells and double-labeled EMS. Similar to our results in intact embryos, we observed that mScarlet::APR-1 was enriched on the anterior cortex of EMS and that mNG::DSH-2 became enriched at the P_2–EMS contact (Figure 6D). In both intact embryos and the cell manipulation experiments, we observed polarization of mScarlet::APR-1 prior to mNG::DSH-2 enrichment, although it is unclear whether this apparent difference in timing is because mNG::APR-1 begins to become excluded from the P_2–EMS contact before DSH-2 arrives, or because the initial recruitment of tagged mNG::DSH-2 is too dim to detect. Therefore, we sought to determine whether one protein affects the other protein's localization.

Dishevelled is required for APR-1/APC polarization

How do these proteins become polarized to different domains at the cell cortex? We next sought to test whether DSH-2/Dishevelled and APR-1/APC affect one another's localization in EMS. An effect of Dishevelled on APR-1/APC localization had been claimed previously, but only using a tagged transgene expressed at undetermined levels alongside wild-type protein (Sugioka *et al.* 2011). We first examined the localization of mNG::DSH-2 when we targeted *apr*-1 by RNAi, and found no change in the fluorescence intensity of mNG::DSH-2 (Figure 7A). Given that we saw no effect, we tested the efficiency of our RNAi conditions in knocking down APR-1 levels by injecting dsRNA targeting *apr-1* into the mNG::APR-1. We observed that the levels of mNG::APR-1 in treated embryos were below detection (Figure S3 in File S1), suggesting

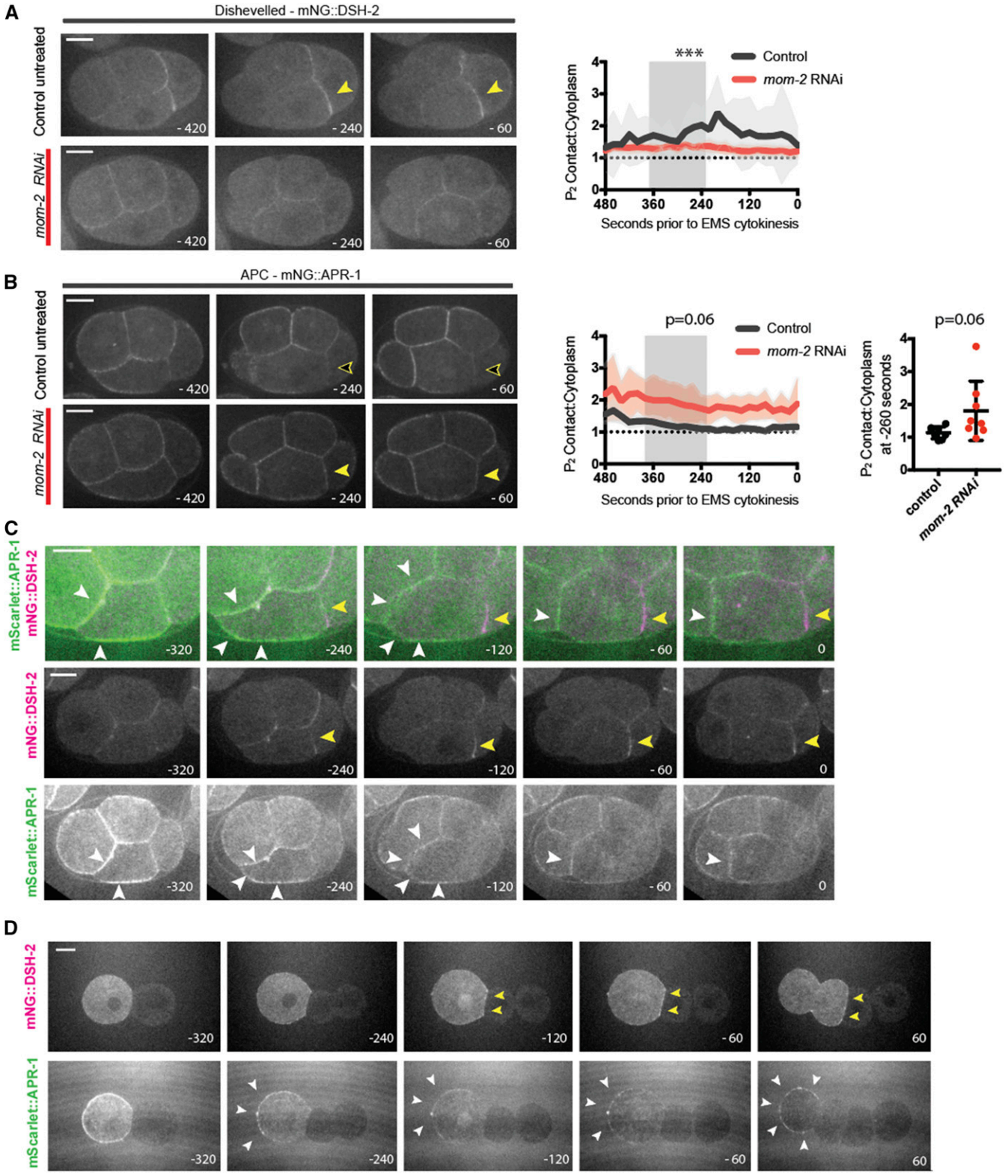

Figure 6 DSH-2/Dishevelled and APR-1/APC are enriched on opposite sides of EMS. (A) Live imaging of embryos expressing mNG::DSH-2 in control and *mom-2* RNAi conditions. Arrowheads point to enrichment of mNG::DSH-2 at P_2–EMS contact site. Control, n =3; *mom-2* RNAi, n =11. Statistical test performed during spindle rotation (−260 sec), *** P = 0.0002. (B) Embryos expressing mNG::APR-1 in control and *mom-2* RNAi-treated conditions. Control, n =8; *mom-2* RNAi, n =8. Statistical test performed during spindle rotation (−260 sec), P = 0.06. (C) mNG::DSH-2 and mScarlet::APR-1 dual-labeled embryos. Top row is a merge zoomed in on the EMS cell and bottom two rows are single channel images from the corresponding time points, n = 5. (D) Recombined cell pair of unlabeled P_2 and dual-labeled mNG::DSH-2 and mScarlet::APR-1-expressing EMS cells. Arrowheads point to enrichments on either side of EMS. n = 6. Bars, 10 μm.

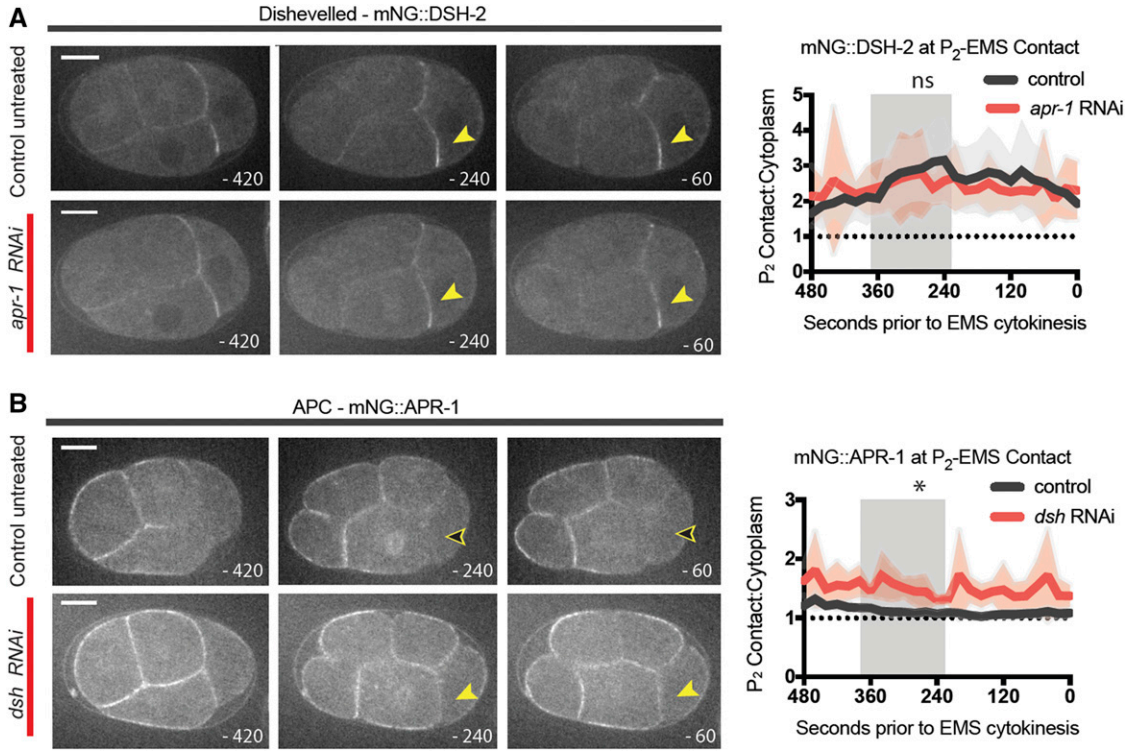

Figure 7 Dishevelled is required for APR-1/APC localization in EMS. (A) Live imaging of embryos expressing mNG::DSH-2 in control and *apr-1* RNAi conditions. Arrowheads point to enrichment of mNG::DSH-2 at P_2–EMS contact site. Control, $n = 7$; *apr-1* RNAi, $n = 7$. Statistical test performed during spindle rotation (−260 sec), $P = 0.18$ (NS). (B) Embryos expressing mNG::APR-1 in control and *dsh* RNAi-treated conditions. Control, $n = 8$; *dsh* RNAi, $n = 8$. Statistical test performed during spindle rotation (−260 sec), * $P = 0.022$. Arrowheads point to enrichments on one side of EMS. Bars, 10 μm.

robust knockdown of APR-1 levels. In contrast to the lack of effect of *apr-1* knockdown on DSH-2 localization, targeting Dishevelled by RNAi did affect mNG::APR-1 localization. When we simultaneously targeted the two major Dishevelled proteins involved in EMS spindle rotation, *dsh-2* and *mig-5*, the cortical domain of mNG::APR-1 expanded and we detected mNG::APR-1 at the P_2–EMS contact, where it is normally excluded (Figure 7B). Co-injected dsRNAs targeting *mig-5* and *dsh-2* resulted in embryonic lethality in all treated embryos (8/8), consistent with the previously reported double-mutant phenotype (Mizumoto and Sawa 2007). This confirmed that Dishevelled proteins are important for natively tagged APR-1 to become localized to the anterior of EMS. These results suggest that cortical Dishevelled is important for excluding mNG::APR-1 from a domain of the posterior cortex of EMS.

Taken together, our results identify Dishevelled and APC homologs as key spindle orientation proteins whose localization within a responding cell *in vivo* is controlled by cell–cell signaling, and the results suggest Wnt-dependent local recruitment of a Dishevelled homolog(s) somehow restricts APR-1/APC to the opposite side of the cell.

Discussion

Mechanistic knowledge of how signaling between cells can direct oriented cell divisions is limited to a handful of contexts, and the generality of these mechanisms is unknown (Werts and Goldstein 2011; Bergstralh *et al.* 2017). Here, we explored how Wnt signaling orients the mitotic spindle using the well-characterized EMS cell division of the *C. elegans* embryo to confirm and extend previous observations on this system. Using a set of new fluorescent protein fusions that we generated via Cas9-triggered homologous recombination, we screened for cortically localized proteins, characterized their dynamics throughout the EMS cell cycle, and performed functional experiments testing interactions between genes genetically implicated in EMS spindle rotation. Although LIN-5/NuMA and DHC-1/dynein were enriched at the P_2–EMS contact in intact embryos, we unexpectedly found that neither protein was enriched in EMS (Figure 3, C and D, and Figure 4B). These data eliminate one specific hypothesis that we had previously considered likely—that LIN-5/NuMA is recruited asymmetrically in EMS by Dishevelled, as is the case in *Drosophila* sensory organ precursor-oriented cell division (Ségalen *et al.* 2010). We found, instead, that LIN-5/NuMA is enriched within P_2 where it contacts EMS (Figure 3C), similar to LGN, which functions as an upstream binding partner of NuMA in many systems (Werts *et al.* 2011). We speculate that LIN-5/NuMA functions in P_2 spindle orientation downstream of MES-1 and GPR-1/2/LGN.

We analyzed other candidate proteins in the Wnt pathway for potential asymmetry during spindle rotation and found that DSH-2/Dishevelled and APR-1/APC were enriched in

the posterior and anterior of EMS, respectively (Figure 6). The asymmetric localization of these cortical cues was dependent on *mom-2*/Wnt signaling, and targeting Dishevelled by RNAi resulted in ectopic APR-1/APC localization at the P_2–EMS contact (Figure 7). Combined with previous genetic data, these results are consistent with the hypothesis that Dishevelled and APC might serve as asymmetric cortical cues for EMS spindle rotation (Sugioka *et al.* 2011; see below).

Using endogenously tagged proteins to screen by localization

We took an unusual approach to test our hypothesis that Wnt signaling directs mitotic spindle positioning by locally recruiting force-generating complexes to the EMS cortex, tagging a "parts list" of gene products required for, or suspected to play a role in, spindle rotation in EMS (Schlesinger *et al.* 1999; Bei *et al.* 2002; Tsou *et al.* 2003; Walston *et al.* 2004; Zhang *et al.* 2008; Liro and Rose 2016). Endogenously tagged versions of these proteins were needed to follow protein dynamics live in specific cells and to determine which proteins are asymmetrically localized in EMS. By using CRISPR-Cas9-triggered homologous recombination to insert genes encoding fluorescent proteins into the endogenous genetic loci of many of our genes of interest, we were able to identify gene products that are asymmetrically localized within EMS. This approach demonstrates the value of localization-based screening, and we expect that larger-scale screens will become feasible as the number of tagged strains generated by the community expands.

Asymmetric localization vs. asymmetric activation

Most well-characterized cases of oriented cell division involve the asymmetric localization of LGN and/or NuMA to a specific region of the cell cortex, toward which the mitotic spindle is pulled (Kotak and Gönczy 2013; di Pietro *et al.* 2016; Bergstralh *et al.* 2017). Together with previous studies, our results indicate that asymmetric localization of GPR-1/2/LGN and/or LIN-5/NuMA is not the mechanism of mitotic spindle positioning in EMS (Werts *et al.* 2011; Figure 3 and Figure 4). However, loss-of-function, temperature-sensitive mutants of *gpa-16*/Gα, *lin-5*/NuMA, and the dynein regulator *dnc-1*/p150 dynactin impair EMS spindle rotation (Tsou *et al.* 2003; Zhang *et al.* 2008; Liro and Rose 2016); suggesting that symmetrically distributed Gα/LGN/NuMA complexes and dynein are important for allowing normal spindle movement and positioning. It is possible that although members of these canonical complexes are not asymmetrically localized, they could be asymmetrically activated or inactivated to generate localized pulling forces. In fact, recent studies in the one-cell-stage *C. elegans* embryo suggest that phosphorylation of LIN-5/NuMA is important for its ability to bind dynein and induce asymmetric spindle positioning (Portegijs *et al.* 2016). However, these sites of phospho-regulation did not appear to affect the function of LIN-5/NuMA in EMS spindle positioning (Portegijs *et al.* 2016), suggesting that either a different mechanism for LIN-5/NuMA activation is important in EMS or that spindle positioning in EMS does not require differential activation of LIN-5/NuMA. The idea that cortical adaptor proteins like LGN and NuMA, dynein, or a regulator of dynein might be locally activated is a difficult hypothesis to test currently given the number of possible regulators and the difficulty of isolating sufficient stage-specific material to perform proteomic methods to identify post-translational modifications.

How might members of the Wnt pathway, Dishevelled and APC, act as positional cues for mitotic spindle positioning?

We showed that by the end of mitotic spindle rotation, DSH-2/Dishevelled and APR-1/APC occupy distinct domains of the EMS cortex, polarized along the anterior–posterior axis (Figure 6). This reciprocal localization pattern is highly reminiscent of Par protein polarity in the one-cell-stage embryo (Cuenca *et al.* 2003). Like Par protein complexes, it is possible that APR-1/APC and/or Dishevelled have downstream effectors that regulate mitotic spindle positioning, and that their cortical asymmetry serves as a spatial cue for mitotic spindle positioning (Grill *et al.* 2001). A recent report demonstrates that, in the asymmetric cell division of the *C. elegans* zygote, APR-1/APC enriched at the anterior cell cortex and inhibits anterior centrosome movements, probably through the stabilization of astral microtubules (Sugioka *et al.* 2017). It is possible that APR-1/APC plays a similar role during EMS division. However, at this point it is unknown if one or both proteins might serve as a sufficient spatial cue for orienting the mitotic spindle.

It is possible that these proteins together provide positional information, or that only one protein plays this role and the other protein functions solely to restrict its localization to one side of EMS. Targeting *apr-1* by RNAi did not decrease mNG::DSH-2 enrichment at the P_2–EMS contact (Figure 7A), but targeting two Dishevelleds (*dsh-2* and *mig-5*) by RNAi caused mNG::APR-1 to no longer be restricted to the anterior cortex of EMS (Figure 7B); suggesting that Dishevelled enrichment on the posterior cortex of EMS is upstream of APR-1/APC localization. This result is consistent with the finding that MIG-5/Dishevelled regulates APR-1/APC localization in asymmetric cell division of the *C. elegans* seam cells (Baldwin *et al.* 2016). However, we were surprised to find mNG::APR-1 polarized at the cell cortex before Dishevelled in double-labeled embryos (Figure 6, C and D). Although we did not detect asymmetrically localized mNG::DSH-2 prior to posterior exclusion of APR-1, mNG::DSH-2 may have been present at levels too low to detect in these experiments.

Neither APC nor Dishevelled contain catalytic domains, therefore it is unlikely that these molecules generate force on astral microtubules directly in the way that a motor protein does. More likely, these proteins either regulate microtubule dynamics or the activity of force-generating complexes within their respective cortical domains. Homologs of APR-1/APC are known to interact with and stabilize microtubules through the microtubule plus-end binding protein EB1 in mammalian cells (Munemitsu *et al.* 1994; Smith *et al.* 1994; Nakamura

et al. 2001; Green *et al.* 2005). In mitotic spindle positioning in budding yeast, Kar9 (a protein with weak homology to APC) and Bim (an EB1 homolog) serve as a link between astral microtubules and myosin motor proteins at the cell cortex (Lee *et al.* 2000; Yeh *et al.* 2000). APC has also been shown to play a role in centrosome anchoring during spindle orientation in *Drosophila* germline stem cells (Yamashita *et al.* 2003) and in the early *Drosophila* embryo (Poulton *et al.* 2013).

There is some evidence in *C. elegans* that APR-1 regulates microtubule plus-end dynamics. Microtubule dwell times are longer at the anterior cortex than in the posterior cortex of EMS during telophase, and this difference is lost when APR-1 is reduced (Sugioka *et al.* 2011). This activity of APR-1 was also reported to cause asymmetry in the number of spindle microtubules in the anterior *vs.* posterior late in the EMS cell cycle, during telophase, and this asymmetry is important for nuclear asymmetry and fate in the resulting EMS daughter cells through differential trafficking of proteins between the nucleus and the cell cortex (Sugioka *et al.* 2011). Because we can now demonstrate APR-1 polarization earlier, during EMS spindle rotation (Figure 5), it is possible that Wnt-dependent localization of APR-1 plays a role in mitotic spindle positioning through the direct regulation of microtubules. Reduction of APR-1 by RNAi was previously shown to have no effect on spindle orientation in EMS (Bei *et al.* 2002), suggesting either no role or a redundant role in spindle orientation. It may be important to note, though, that such a reduction of APR-1 is the opposite of what happens in the absence of Wnt signaling, which is that the domain of APR-1 expands to the posterior cortex of EMS (Figure 6) (Sugioka *et al.* 2011). It is possible that when Wnt signaling is reduced, microtubules are inappropriately stabilized by APR-1 on both sides of EMS, preventing proper spatial positioning.

APR-1/APC or Dishevelled might serve as positional cues for mitotic spindle positioning by recruiting activators or inhibitors of motor proteins. LET-99 is a DEP domain-containing protein, and an antagonist of the Gα/LGN/NuMA force-generating complex in the one-cell-stage *C. elegans* embryo (Tsou *et al.* 2003). LET-99 is required for spindle positioning in EMS (Liro and Rose 2016). In intact four-cell-stage embryos, LET-99 is localized cortically and is reduced at the P_2–EMS contact in a similar pattern to APR-1/APC (Tsou *et al.* 2003; Werts *et al.* 2011). It is possible that APR-1/APC regulates LET-99 to tune pulling forces on one side of the EMS cortex. Dishevelled might also recruit proteins that modulate motor activity. Hypotheses about how Dishevelled and APC might act as positional cues for mitotic spindle positioning would be greatly informed by knowledge of the direction of force imbalances generated on the mitotic spindle to facilitate positioning within EMS. WRM-1/β-catenin has also been reported to be a regulator of EMS spindle rotation, and is normally found on the anterior cortex of EMS (Kim *et al.* 2013). WRM-1/β-catenin may act in parallel to APR-1/APC, which has a similar localization pattern, or its absence from the posterior of EMS could facilitate the interaction of Dishevelled with microtubules.

In conclusion, we found DSH-2/Dishevelled and APR-1/APC, but not Lin-5/NuMA and DHC-1/dynein, to be asymmetrically localized at the EMS cortex. It will be interesting to explore a possible mechanism for mitotic spindle positioning that does not appear to rely on the asymmetric localization of the conserved Gα/LGN/NuMA protein complex. We speculate that there may be more cases where signaling pathway proteins serve as spatial cues for mitotic spindle positioning independent of Gα/LGN/NuMA localization.

Acknowledgments

We thank Alicia Chen and Terrence Wong for materials and plates. We thank WormBase and the *Caenorhabditis* Genetics Center. WormBase is supported by National Institutes of Health grant U41 HG-002223, the U.K. Medical Research Council, and the U.K. Biotechnology and Biological Sciences Research Council. The *Caenorhabditis* Genetics Center is funded by the National Institutes of Health Office of Research Infrastructure Programs grant P40 OD-010440. This work was supported by a U.S. National Science Foundation graduate research fellowship (J.K.H.), National Institutes of Health T32 GM-119999 (A.M.R.), National Institutes of Health T32 CA-009156 (D.J.D. and A.M.P.), a Howard Hughes postdoctoral fellowship from the Helen Hay Whitney Foundation and National Institutes of Health K99 GM-115964 (D.J.D.), National Institutes of Health F32 GM-115151 and American Cancer Society postdoctoral fellowship PF-16-030 - DDC (A.M.P), and National Science Foundation IOS 0917726 and National Institutes of Health R01 GM-083071 (B.G.).

Author contributions: Conceptualization, J.K.H. and B.G.; investigation, J.K.H. and A.M.R.; reagents and methods development, J.K.H., A.M.P., and D.J.D.; writing of original draft, J.K.H. and B.G.; writing (review and editing), J.K.H., A.M.P., D.J.D., and B.G.; funding acquisition, B.G.; resources, B.G.; supervision, B.G.

Literature Cited

Ali, M. Y., and S. S. Siddiqui, 2000 cDNA cloning and expression of a C-terminus motor kinesin-like protein KLP-17, involved in chromosomal movement in *Caenorhabditis elegans*. Biochem. Biophys. Res. Commun. 267: 643–650.

Baldwin, A. T., A. M. Clemons, and B. T. Phillips, 2016 Unique and redundant β-catenin regulatory roles of two Dishevelled paralogs during *C. elegans* asymmetric cell division. J. Cell Sci. 129: 983–993.

Barbosa, D. J., J. Duro, B. Prevo, D. K. Cheerambathur, A. X. Carvalho *et al.*, 2017 Dynactin binding to tyrosinated microtubules promotes centrosome centration in *C. elegans* by enhancing dynein-mediated organelle transport. PLoS Genet. 13: e1006941.

Bei, Y., J. Hogan, L. A. Berkowitz, M. C. Soto, C. E. Rocheleau *et al.*, 2002 SRC-1 and Wnt signaling act together to specify endoderm and to control cleavage orientation in early *C. elegans* embryos. Dev. Cell 3: 113–125.

Bergstralh, D. T., N. S. Dawney, and D. St Johnston, 2017 Spindle orientation: a question of complex positioning. Development 144: 1137–1145.

Berkowitz, L. A., and S. Strome, 2000 MES-1, a protein required for unequal divisions of the germline in early C. elegans embryos, resembles receptor tyrosine kinases and is localized to the boundary between the germline and gut cells. Development 127: 4419–4431.

Bossinger, O., A. Klebes, C. Segbert, C. Theres, and E. Knust, 2001 Zonula adherens formation in *Caenorhabditis elegans* requires *dlg-1*, the homologue of the *Drosophila* gene *discs large*. Dev. Biol. 230: 29–42.

Chien, S.-C. J., M. Gurling, C. Kim, T. Craft, W. Forrester *et al.*, 2015 Autonomous and nonautonomous regulation of Wnt-mediated neuronal polarity by the *C. elegans* Ror kinase CAM-1. Dev. Biol. 404: 55–65.

Cockell, M. M., K. Baumer, and P. Gönczy, 2004 *lis-1* is required for dynein-dependent cell division processes in *C. elegans* embryos. J. Cell Biol. 117: 4571–4582.

Couwenbergs, C., J. C. Labbe, M. Goulding, T. Marty, B. Bowerman *et al.*, 2007 Heterotrimeric G protein signaling functions with dynein to promote spindle positioning in *C. elegans*. J. Cell Biol. 179: 15–22.

Cuenca, A. A., A. Schetter, D. Aceto, K. Kemphues, and G. Seydoux, 2003 Polarization of the *C. elegans* zygote proceeds via distinct establishment and maintenance phases. Development 130: 1255–1265.

Delaunay, D., V. Cortay, D. Patti, K. Knoblauch, and C. Dehay, 2014 Mitotic spindle asymmetry: a Wnt/PCP-regulated mechanism generating asymmetrical division in cortical precursors. Cell Rep. 6: 400–414.

Dickinson, D. J., J. D. Ward, D. J. Reiner, and B. Goldstein, 2013 Engineering the *Caenorhabditis elegans* genome using Cas9-triggered homologous recombination. Nat. Methods 10: 1028–1034.

Dickinson, D. J., A. M. Pani, J. K. Heppert, C. D. Higgins, and B. Goldstein, 2015 Streamlined genome engineering with a self-excising drug selection cassette. Genetics 200: 1035–1049.

di Pietro, F., A. Echard, and X. Morin, 2016 Regulation of mitotic spindle orientation: an integrated view. EMBO Rep. 17: 1106–1130.

Dudley, N. R., J. C. Labbé, and B. Goldstein, 2002 Using RNA interference to identify genes required for RNA interference. Proc. Natl. Acad. Sci. USA 99: 4191–4196.

Edgar, L. G., and B. Goldstein, 2012 Culture and manipulation of embryonic cells. Methods Cell Biol. 107: 151–175.

Firestein, B. L., and C. Rongo, 2001 DLG-1 is a MAGUK similar to SAP97 and is required for adherens junction formation. Mol. Biol. Cell 12: 3465–3475.

Galli, M., J. Muñoz, V. Portegijs, M. Boxem, S. W. Grill *et al.*, 2011 aPKC phosphorylates NuMA-related LIN-5 to position the mitotic spindle during asymmetric division. Nat. Cell Biol. 13: 1132–1138.

Gassmann, R., A. Essex, J. S. Hu, P. S. Maddox, F. Motegi *et al.*, 2008 A new mechanism controlling kinetochore-microtubule interactions revealed by comparison of two dynein-targeting components: SPDL-1 and the Rod/Zwilch/Zw10 complex. Genes Dev. 22: 2385–2399.

Gillies, T. E., and C. Cabernard, 2011 Cell division orientation in animals. Curr. Biol. 21: R599–R609.

Gloerich, M., J. M. Bianchini, K. A. Siemers, D. J. Cohen, and W. J. Nelson, 2017 Cell division orientation is coupled to cell-cell adhesion by the E-cadherin/LGN complex. Nat. Commun. 8: 13996.

Goldstein, B., 1992 Induction of gut in *Caenorhabditis elegans* embryos. Nature 357: 255–257.

Goldstein, B., 1993 Establishment of gut fate in the E lineage of C. elegans: the roles of lineage-dependent mechanisms and cell interactions. Development 118: 1267–1277.

Goldstein, B., 1995a An analysis of the response to gut induction in the C. elegans embryo. Development 121: 1227–1236.

Goldstein, B., 1995b Cell contacts orient some cell division axes in the Caenorhabditis elegans embryo. J. Cell Biol. 129: 1071–1080.

Goldstein, B., H. Takeshita, K. Mizumoto, and H. Sawa, 2006 Wnt signals can function as positional cues in establishing cell polarity. Dev. Cell 10: 391–396.

Gönczy, P., S. Pichler, M. Kirkham, and A. A. Hyman, 1999 Cytoplasmic dynein is required for distinct aspects of MTOC positioning, including centrosome separation, in the one cell stage *Caenorhabditis elegans* embryo. J. Cell Biol. 147: 135–150.

Gotta, M., and J. Ahringer, 2001 Distinct roles for Gα and Gβγ in regulating spindle position and orientation in *Caenorhabditis elegans* embryos. Nat. Cell Biol. 3: 297–300.

Green, J. L., T. Inoue, and P. W. Sternberg, 2007 The *C. elegans* ROR receptor tyrosine kinase, CAM-1, non-autonomously inhibits the Wnt pathway. Development 134: 4053–4062.

Green, R. A., R. Wollman, and K. B. Kaplan, 2005 APC and EB1 function together in mitosis to regulate spindle dynamics and chromosome alignment. Mol. Biol. Cell 16: 4609–4622.

Grill, S. W., and A. A. Hyman, 2005 Spindle positioning by cortical pulling forces. Dev. Cell 8: 461–465.

Grill, S. W., P. Gonczy, E. H. K. Stelzer, and A. A. Hyman, 2001 Polarity controls forces governing asymmetric spindle positioning in the *Caenorhabditis elegans* embryo. Nature 409: 630–633.

Grill, S. W., J. Howard, E. Schäffer, E. H. K. Stelzer, and A. A. Hyman, 2003 The distribution of active force generators controls mitotic spindle position. Science 301: 518–521.

Habib, S. J., B. C. Chen, F. C. Tsai, K. Anastassiadis, T. Meyer *et al.*, 2013 A localized Wnt signal orients asymmetric stem cell division in vitro. Science 339: 1445–1448.

Han, X., K. Adames, E. M. E. Sykes, and M. Srayko, 2015 The KLP-7 residue S546 is a putative Aurora kinase site required for microtubule regulation at the centrosome in *C. elegans*. PLoS One 10: e0132593.

Hawkins, N. C., G. Garriga, and C. T. Beh, 2003 Creating precise GFP fusions in plasmids using yeast homologous recombination. Biotechniques 34: 74–78, 80.

Hawkins, N. C., G. C. Ellis, B. Bowerman, and G. Garriga, 2005 MOM-5 frizzled regulates the distribution of DSH-2 to control *C. elegans* asymmetric neuroblast divisions. Dev. Biol. 284: 246–259.

Inaba, M., H. Yuan, V. Salzmann, M. T. Fuller, and Y. M. Yamashita, 2010 E-cadherin is required for centrosome and spindle orientation in *Drosophila* male germline stem cells. PLoS One 5: e12473.

Kim, H. T., K. S. Ishidate, M. Ghanta, D. Seth, D. Conte *et al.*, 2014 A co-CRISPR strategy for efficient genome editing in *Caenorhabditis elegans*. Genetics 197: 1069–1080.

Kim, S., T. Ishidate, R. Sharma, M. C. Soto, D. Conte, Jr. *et al.*, 2013 Wnt and CDK-1 regulate cortical release of WRM-1/β-catenin to control cell division orientation in early *Caenorhabditis elegans* embryos. Proc. Natl. Acad. Sci. USA 110: E918–E927.

Kiyomitsu, T., and I. M. Cheeseman, 2012 Chromosome- and spindle-pole-derived signals generate an intrinsic code for spindle position and orientation. Nat. Cell Biol. 14: 311–317.

Kiyomitsu, T., and I. M. Cheeseman, 2013 Cortical dynein and asymmetric membrane elongation coordinately position the spindle in anaphase. Cell 154: 391–402 (erratum: Cell 154: 1401).

Kotak, S., and P. Gönczy, 2013 Mechanisms of spindle positioning: cortical force generators in the limelight. Curr. Opin. Cell Biol. 25: 741–748.

Lechler, T., and E. Fuchs, 2005 Asymmetric cell divisions promote stratification and differentiation of mammalian skin. Nature 437: 275–280.

Lee, L., J. S. Tirnauer, J. Li, S. C. Schuyler, J. Y. Liu *et al.*, 2000 Positioning of the mitotic spindle by a cortical-microtubule capture mechanism. Science 287: 2260–2262.

Le Grand, F., A. E. Jones, V. Seale, A. Scimè, and M. A. Rudnicki, 2009 Wnt7a activates the planar cell polarity pathway to drive the symmetric expansion of satellite stem cells. Cell Stem Cell 4: 535–547.

Liro, M. J., and L. S. Rose, 2016 Mitotic spindle positioning in the EMS cell of *Caenorhabditis elegans* requires LET-99 and LIN-5/NuMA. Genetics 204: 1177–1189.

Lorson, M. A., H. R. Horvitz, and S. van den Heuvel, 2000 Lin-5 is a novel component of the spindle apparatus required for chromosome segregation and cleavage plane specification in *Caenorhabditis elegans*. J. Cell Biol. 148: 73–86.

Lu, M. S., and C. A. Johnston, 2013 Molecular pathways regulating mitotic spindle orientation in animal cells. Development 140: 1843–1856.

Malone, C. J., L. Misner, M. Le Bot, M.-C. Tsai, J. M. Campbell *et al.*, 2003 The *C. elegans* hook protein, ZYG-12, mediates the essential attachment between the centrosome and nucleus. Cell 115: 825–836.

Marston, D. J., C. D. Higgins, K. A. Peters, T. D. Cupp, D. J. Dickinson *et al.*, 2016 MRCK-1 drives apical constriction in *C. elegans* by linking developmental patterning to force generation. Curr. Biol. 26: 2079–2089.

McMahon, L., R. Legouis, J. L. Vonesch, and M. Labouesse, 2001 Assembly of *C. elegans* apical junctions involves positioning and compaction by LET-413 and protein aggregation by the MAGUK protein DLG-1. J. Cell Biol. 114: 2265–2277.

Merdes, A., K. Ramyar, J. D. Vechio, and D. W. Cleveland, 1996 A complex of NuMA and cytoplasmic dynein is essential for mitotic spindle assembly. Cell 87: 447–458.

Mizumoto, K., and H. Sawa, 2007 Cortical β-catenin and APC regulate asymmetric nuclear β-catenin localization during asymmetric cell division in *C. elegans*. Dev. Cell 12: 287–299.

Munemitsu, S., B. Souza, O. Müller, I. Albert, B. Rubinfeld *et al.*, 1994 The APC gene product associates with microtubules *in vivo* and promotes their assembly *in vitro*. Cancer Res. 54: 3676–3681.

Nakamura, M., X. Z. Zhou, and K. P. Lu, 2001 Critical role for the EB1 and APC interaction in the regulation of microtubule polymerization. Curr. Biol. 11: 1062–1067.

Nguyen-Ngoc, T., K. Afshar, and P. Gönczy, 2007 Coupling of cortical dynein and Gα proteins mediates spindle positioning in *Caenorhabditis elegans*. Nat. Cell Biol. 9: 1294–1302.

Oegema, K., A. Desai, S. Rybina, M. Kirkham, and A. A. Hyman, 2001 Functional analysis of kinetochore assembly in *Caenorhabditis elegans*. J. Cell Biol. 153: 1209–1226.

Paix, A., Y. Wang, H. E. Smith, C.-Y. Lee, D. Calidas *et al.*, 2014 Scalable and versatile genome editing using linear DNAs with microhomology to Cas9 sites in *Caenorhabditis elegans*. Genetics 198: 1347–1356.

Park, D. H., and L. S. Rose, 2008 Dynamic localization of LIN-5 and GPR-1/2 to cortical force generation domains during spindle positioning. Dev. Biol. 315: 42–54.

Park, F. D., J. R. Tenlen, and J. R. Priess, 2004 *C. elegans* MOM-5/frizzled functions in MOM-2/Wnt-independent cell polarity and is localized asymmetrically prior to cell division. Curr. Biol. 14: 2252–2258.

Peyre, E., F. Jaouen, M. Saadaoui, L. Haren, A. Merdes *et al.*, 2011 A lateral belt of cortical LGN and NuMA guides mitotic spindle movements and planar division in neuroepithelial cells. J. Cell Biol. 193: 141–154.

Portegijs, V., L.-E. Fielmich, M. Galli, R. Schmidt, J. Muñoz *et al.*, 2016 Multisite phosphorylation of NuMA-related LIN-5 controls mitotic spindle positioning in *C. elegans*. PLoS Genet. 12: e1006291.

Poulton, J. S., F. W. Mu, D. M. Roberts, and M. Peifer, 2013 APC2 and Axin promote mitotic fidelity by facilitating centrosome separation and cytoskeletal regulation. Development 140: 4226–4236.

Rappaport, R., 1961 Experiments concerning the cleavage stimulus in sand dollar eggs. J. Exp. Zool. 148: 81–89.

Rocheleau, C. E., W. D. Downs, R. Lin, C. Wittmann, Y. Bei *et al.*, 1997 Wnt signaling and an APC-related gene specify endoderm in early C. elegans embryos. Cell 90: 707–716.

Schlesinger, A., C. A. Shelton, J. N. Maloof, M. Meneghini, and B. Bowerman, 1999 Wnt pathway components orient a mitotic spindle in the early *Caenorhabditis elegans* embryo without requiring gene transcription in the responding cell. Genes Dev. 13: 2028–2038.

Schmidt, D. J., D. J. Rose, W. M. Saxton, and S. Strome, 2005 Functional analysis of cytoplasmic dynein heavy chain in *Caenorhabditis elegans* with fast-acting temperature- sensitive mutations. Mol. Biol. Cell 16: 1200–1212.

Ségalen, M., C. A. Johnston, C. A. Martin, J. G. Dumortier, K. E. Prehoda *et al.*, 2010 The Fz-Dsh planar cell polarity pathway induces oriented cell division via Mud/NuMA in *Drosophila* and zebrafish. Dev. Cell 19: 740–752.

Seldin, L., N. D. Poulson, H. P. Foote, and T. Lechler, 2013 NuMA localization, stability, and function in spindle orientation involve 4.1 and Cdk1 interactions. Mol. Biol. Cell 24: 3651–3662.

Siller, K. H., and C. Q. Doe, 2008 Lis1/dynactin regulates metaphase spindle orientation in *Drosophila* neuroblasts. Dev. Biol. 319: 1–9.

Siller, K. H., C. Cabernard, and C. Q. Doe, 2006 The NuMA-related Mud protein binds Pins and regulates spindle orientation in *Drosophila* neuroblasts. Nat. Cell Biol. 8: 594–600.

Singh, D., and C. Pohl, 2014 A function for the midbody remnant in embryonic patterning. Commun. Integr. Biol. 7: e28533.

Skop, A. R., and J. G. White, 1998 The dynactin complex is required for cleavage plane specification in early *Caenorhabditis elegans* embryos. Curr. Biol. 8: 1110–1116.

Smith, K. J., D. B. Levy, P. Maupin, T. D. Pollard, B. Vogelstein *et al.*, 1994 Wild-type but not mutant APC associates with the microtubule cytoskeleton. Cancer Res. 54: 3672–3675.

Smith, P., M. Azzam, and L. Hinck, 2017 Extracellular regulation of the mitotic spindle and fate determinants driving asymmetric cell division. Results Probl. Cell Differ. 61: 351–373.

Song, S., B. Zhang, H. Sun, X. Li, Y. Xiang *et al.*, 2010 A Wnt-Frz/Ror-Dsh pathway regulates neurite outgrowth in *Caenorhabditis elegans*. PLoS Genet. 6: e1001056.

Srinivasan, D. G., R. M. Fisk, H. Xu, and S. van den Heuvel, 2003 A complex of LIN-5 and GPR proteins regulates G protein signaling and spindle function in *C. elegans*. Genes Dev. 17: 1225–1239.

Sugioka, K., K. Mizumoto, and H. Sawa, 2011 Wnt regulates spindle asymmetry to generate asymmetric nuclear β-catenin in *C. elegans*. Cell 146: 942–954.

Sugioka, K., L.-E. Fielmich, K. Mizumoto, B. Bowerman, S. van den Heuvel *et al.*, 2017 The tumor suppressor APC is an attenuator of spindle-pulling forces during C. elegans asymmetric cell division. bioRxiv Available at: https://doi.org/10.1101/157404.

Tame, M., J. Raaijmakers, B. van den Broek, A. Lindqvist, K. Jalink *et al.*, 2014 Astral microtubules control redistribution of dynein at the cell cortex to facilitate spindle positioning. Cell Cycle 13: 1162–1170.

Thorpe, C. J., A. Schlesinger, J. C. Carter, and B. Bowerman, 1997 Wnt signaling polarizes an early C. elegans blastomere to distinguish endoderm from mesoderm. Cell 90: 695–705.

Tsou, M. F., A. Hayashi, and L. S. Rose, 2003 LET-99 opposes G /GPR signaling to generate asymmetry for spindle positioning in response to PAR and MES-1/SRC-1 signaling. Development 130: 5717–5730.

Walston, T., C. Tuskey, L. Edgar, N. Hawkins, G. Ellis *et al.*, 2004 Multiple Wnt signaling pathways converge to orient the mitotic spindle in early *C. elegans* embryos. Dev. Cell 7: 831–841.

Werts, A. D., and B. Goldstein, 2011 How signaling between cells can orient a mitotic spindle. Semin. Cell Dev. Biol. 22: 842–849.

Werts, A. D., M. Roh-Johnson, and B. Goldstein, 2011 Dynamic localization of *C. elegans* TPR-GoLoco proteins mediates mitotic spindle orientation by extrinsic signaling. Development 138: 4411–4422.

Williams, S. E., S. Beronja, H. A. Pasolli, and E. Fuchs, 2011 Asymmetric cell divisions promote Notch-dependent epidermal differentiation. Nature 470: 353–358.

Wong, H.-C., A. Bourdelas, A. Krauss, H.-J. Lee, Y. Shao *et al.*, 2003 Direct binding of the PDZ domain of Dishevelled to a conserved internal sequence in the C-terminal region of Frizzled. Mol. Cell 12: 1251–1260.

Woodard, G. E., N.-N. Huang, H. Cho, T. Miki, G. G. Tall *et al.*, 2010 Ric-8A and Gi alpha recruit LGN, NuMA, and dynein to the cell cortex to help orient the mitotic spindle. Mol. Cell. Biol. 30: 3519–3530.

Xia, J., J. M. Swiercz, I. Bañón-Rodríguez, I. Matković, G. Federico *et al.*, 2015 Semaphorin-plexin signaling controls mitotic spindle orientation during epithelial morphogenesis and repair. Dev. Cell 33: 299–313.

Yamashita, Y. M., D. L. Jones, and M. T. Fuller, 2003 Orientation of asymmetric stem cell division by the APC tumor suppressor and centrosome. Science 301: 1547–1550.

Yeh, E., C. Yang, E. Chin, P. Maddox, E. D. Salmon *et al.*, 2000 Dynamic positioning of mitotic spindles in yeast: role of microtubule motors and cortical determinants. Mol. Biol. Cell 11: 3949–3961.

Yoshiura, S., N. Ohta, and F. Matsuzaki, 2012 Tre1 GPCR signaling orients stem cell divisions in the *Drosophila* central nervous system. Dev. Cell 22: 79–91.

Yuzawa, S., S. Kamakura, Y. Iwakiri, J. Hayase, and H. Sumimoto, 2011 Structural basis for interaction between the conserved cell polarity proteins Inscuteable and Leu-Gly-Asn repeat-enriched protein (LGN). Proc. Natl. Acad. Sci. USA 108: 19210–19215.

Zhang, H., A. R. Skop, and J. G. White, 2008 Src and Wnt signaling regulate dynactin accumulation to the P2-EMS cell border in *C. elegans* embryos. J. Cell Biol. 121: 155–161.

Zheng, Z., H. Zhu, Q. Wan, J. Liu, Z. Xiao *et al.*, 2010 LGN regulates mitotic spindle orientation during epithelial morphogenesis. J. Cell Biol. 189: 275–288.

Communicating editor: M. Sundaram

Figure S1. Later stage embryos and animals

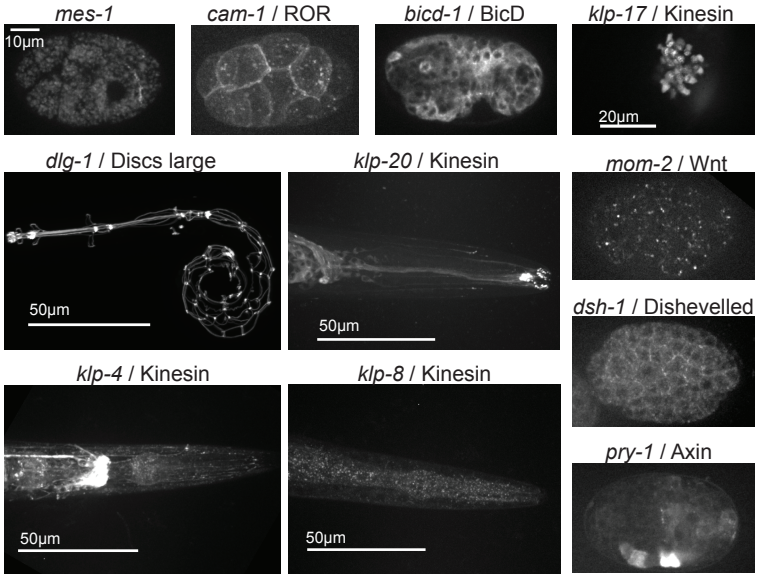

Supplemental Figure 1. Later stage embryos and animals for strains with no detectable fluorescent signal at the four-cell stage. mes-1, cam-1, bicd-1, mom-2, dsh-1, pry-1: multi-cell stage embryos. klp-17: sperm. dlg-1: whole L1 larva. klp-20, klp-4, klp-8: pharyngeal region. Images are maximum intensity projections of multiple Z planes. Scale bar lengths are indicated on panels.

Figure S2. Live imaging of mNG::APR-1 embryos

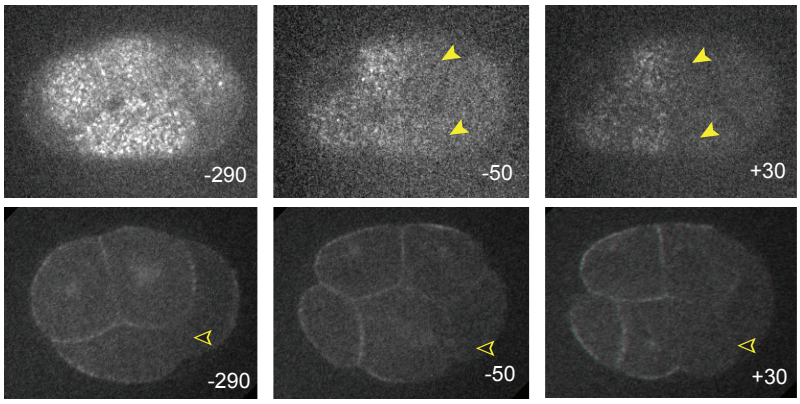

Supplemental Figure 2. Live imaging of stage-matched mNG::APR-1 embryos: cortical view (top row) and midplane (bottom row). Yellow-filled arrowheads highlight the domain of mNG::APR-1 cortical puncta receding towards the anterior, in both ABp (top arrowhead) and EMS (bottom arrowhead). Black-filled arrowheads highlight absence of midplane mNG::APR-1 at the P2:EMS. Scale bars = 10μm.

Figure S3. APR-1 RNAi Knockdown

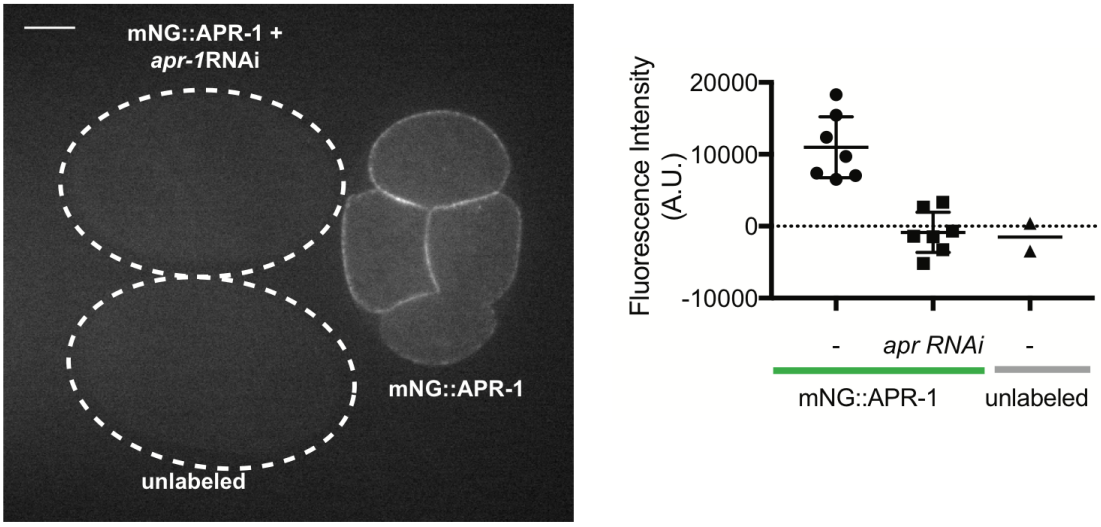

Supplemental Figure 3. Quantification of RNAi knockdown from dsRNA targeting APR-1. The image shows three embryos: unlabeled, untreated; mNG::APR-1, untreated; and mNG::APR-1, treated with dsRNA targeting APR-1. Quantification is from paired imaging of mNG::APR-1 with and without dsRNA treatment, and two cases of triple mounts which included an unlabeled, untreated embryo. Zero represents the off-embryo background level of fluorescence. Scale bars = 10μm.

Table S1. Previous tools for protein localization in *C. elegans* embryos

Proteins		Previous tools for protein localization in *C. elegans* embryos					New tools for protein localization
		Antibodies, fixed embryos	Transgenes			Endogenous tags	Endogenous tags
Protein	Worm name		fully rescuing	partially rescuing	ability to rescue not tested		
Wnt	MOM-2				Song et al., 2010		LP559
Frizzled	MOM-5				Park et al., 2004		LP184* , LP697
GSK3β	GSK-3						LP538
Dishevelled	DSH-2	Walston et al., 2004; Hawkins et al., 2005	Hawkins et al., 2003				LP228*
Dishevelled	MIG-5						LP728*
Dishevelled	DSH-1						LP705
APC	APR-1				Sugioka et al., 2011		LP435*
Axin	PRY-1						LP713
Ror	CAM-1	Chien et al., 2015					LP530
RTK-like	MES-1	Berkowitz and Strome, 2000; Bei et al., 2002					LP527
Dynactin^{p150}	DNC-1	Skop, et al., 1998, Zhang et al., 2008		Zhang et al., 2008			LP563*
NuMA	LIN-5	Lorson et al., 2000					LP585*
Dynein heavy chain	DHC-1	Gonczy et al., 1999, Schmidt et al., 2005			Gassmann et al., 2008	Barbosa et al., 2017	LP560*
NDE1 (NudE)	NUD-2						LP439
Bicaudal D	BICD-1						LP451
Lisencephaly	LIS-1	Cockell et al., 2004		Cockell et al., 2004			LP591*
Discs large	DLG-1	Bossinger et al., 2001	McMahon et al., 2001		Firestein et al., 2001		LP598
MCAK (Kinesin-like)	KLP-7	Oegema et al., 2001	Han et al., 2015				LP447
NCD, Kar3 (Kinesin-like)	KLP-17						LP443
KIF21B (Kinesin-like)	KLP-12						LP521
Kinesin-like	KLP-20						LP608
KHC-73, KIF1A (Kinesin-like)	KLP-4						LP600
Kinesin-like	KLP-8						LP604

Supplemental Table 1. Previous tools for protein localization in C. elegans embryos. Dark red text represents tools that were not detectable at the 4-cell stage. Strains for which embryonic lethality was quantified on average as less than 1% are labeled with a star (*) – See Supplemental Table 3A.

Table S2. List of *C. elegans* strains generated

Mammalian gene name	*C. elegans* gene name	Tag location	Strain Name	Genotype	Method
Wnt	*mom-2*	3'end	LP559	mom-2(cp267[mom-2::mNG-C1^3xFlag]) V	2
Frizzled	*mom-5*	3'end	LP697	mom-5(cp367[mom-5::mNG-C1^3xFlag]) I	3
Frizzled	*mom-5*	3'end	LP184	mom-5(cp31[mom-5::YPET + LoxP]) I	1
Gsk3	*gsk-3*	3'end	LP538	gsk-3(cp251[gsk-3::mNG-C1^3xFlag])	3
Dishevelled	*dsh-2*	5'end	LP228	dsh-2(cp51[mNeonGreen::dsh-2]) II	1
Dishevelled	*mig-5*	5'end	LP728	mig-5(cp385[mNG-GLO^AID::mig-5]) II	3
Dishevelled	*dsh-1*	internal	LP705	dsh-1(cp375[dsh-1DIX::mNG-C1^3xFlag::PDZ,DEP]) II	3
APC	*apr-1*	5'end	LP435	apr-1(cp166[mNG-C1^3xFlag::apr-1]) I	3
Axin	*pry-1*	3'end	LP713	pry-1(cp383[pry-1::mNG-C1^3xFlag]) I	3
Ror	*cam-1*	3'end	LP530	cam-1(cp243[cam-1::mNG-C1^3xFlag])	3
RTK-like	*mes-1*	3'end	LP527	mes-1(cp240[mes-1::mNG-C1^3xFlag]	3
p150 Dynactin	*dnc-1*	3'end	LP563	dnc-1(cp271[dnc::mNG-C1^3xFlag]) IV	3
NuMA	*lin-5*	3'end	LP585	lin-5(cp288[lin-5::mNG-C1^3xFlag]) II	3
Dynein	*dhc-1*	3'end	LP560	dhc-1(cp268[dhc::mNG-C1^3xFlag]) I	3
NudE	*nud-2*	3'end	LP439	nud-2(cp170[nud-2::mNG-C1^3xFlag]) I	3
BicaudalD	*bicd-1*	5'end	LP451	bicd-1(cp180[mNG-C1^3xFlag::bicd-1]) IV	3
Lis1	*lis-1*	3'end	LP591	lis-1(cp294[lis-1::mNG-C1^3xFlag]) III	3
Discs large	*dlg-1*	3'end	LP598	dlg-1(cp301[dlg-1::mNG-C1^3xFlag]) X	3
MCAK	*klp-7*	3'end	LP447	klp-7(cp178[klp-7::mNG-C1^3xFlag]) III	3
Kinesin	*klp-17*	3'end	LP443	klp-17(cp174[klp-17::mNG-C1^3xFlag]) II	3
Kinesin	*klp-12*	3'end	LP521	klp-12(cp234[klp-12::mNG-C1^3xFlag])	3
Kinesin	*klp-20*	3'end	LP608	klp-20(cp311[klp-20::mNG-C1^3xFlag]) III	3
Kinesin	*klp-4*	3'end	LP600	klp-4(cp303[klp-4::mNG-C1^3xFlag]) X	3
Kinesin	*klp-8*	3'end	LP604	klp-8(cp307[klp-8::mNG-C1^3xFlag]) X	3
Dishevelled and APC	*dsh-2; apr-1*	5'end; 5'end	LP776	apr-1(cp397[mSc-C1::apr-1]) I; dsh-2(cp51[mNeonGreen::dsh-2]) II	3

Supplemental Table 2. List of C. elegans strains generated. Method refers to the method used to generate the knock-ins 1 = method of Dickinson et al., 2013, 2 = Paix et al., 2014, 3 = Dickinson et al., 2015.

Table S3.

3A Lethality for strains used

	Strain	Avg. % lethality	n (replicates)
wild type	N2	0.89	1164 (3)
mom-5 3'end	LP184	0.27	442 (3)
dsh-2 5'end	LP228	0.29	1044 (3)
mig-5 5'end	LP728	0.12	749 (2)
apr-1 5'end	LP435	0.31	1278 (3)
lin-5 3'end	LP585	0.28	1264 (3)
dhc-1 3'end	LP560	0.81	909 (3)
dnc-1 3'end	LP563	0.80	721 (3)
lis-1 3'end	LP591	0.26	1112 (3)

3B sgRNA primers

Target	**Target Sequence**
mom-2 3'end	ACATACATTGGGCCCAATAT GTTTTAGAGCTAGAAATAGCAAGT
mom-5 3'end	TGACCTCGAAGAGAGTGCC GTTTTAGAGCTAGAAATAGCAAGT
mom-5 3'end	TGTACCTGCTCATGTTGATC GTTTTAGAGCTAGAAATAGCAAGT
gsk-3 3'end	CGGTGATGTGGCTGGCCCAT GTTTTAGAGCTAGAAATAGCAAGT
dsh-2 5'end	CGTCAAATGATGAATCAAT GTTTTAGAGCTAGAAATAGCAAGT
mig-5 5'end	CTGCAGTCTGATGTGCATGGGTTTTAGAGCTAGAAATAGCAAGT
dsh-1 internal	TCAAGGCTCATAGAGGACTC GTTTTAGAGCTAGAAATAGCAAGT
apr-1 5'end	TGAGTAGATTCCACTTCCACGTTTTAGAGCTAGAAATAGCAAGT
pry-1 3'end	ATAATCCCACTATCGGAGCT GTTTTAGAGCTAGAAATAGCAAGT
cam-1 3'end	AGAGGATGGTGATTCTGATT GTTTTAGAGCTAGAAATAGCAAGT
mes-1 3'end	GGGTGTATTCATCTAAACCG GTTTTAGAGCTAGAAATAGCAAGT
dnc-1 3'end	CTACCACACGATTCCCCACTGTTTTAGAGCTAGAAATAGCAAGT
lin-5 3'end	GTCCAAGAAAAAGAACCGTC GTTTTAGAGCTAGAAATAGCAAGT
dhc-1 3'end	AGACGATTAGAGAGTTGAGTGTTTTAGAGCTAGAAATAGCAAGT
nud-2 3'end	CCGTGTCGTTGTAAGATGAC GTTTTAGAGCTAGAAATAGCAAGT
bicd-1 5'end	CAATTCTGATTCAGCCATTG GTTTTAGAGCTAGAAATAGCAAGT
lis-1 3'end	ATGGAGAATATTTCGGTCAA GTTTTAGAGCTAGAAATAGCAAGT
dlg-1 3'end	TAATGACGTGGCACCCAAAT GTTTTAGAGCTAGAAATAGCAAGT
klp-7 3'end	AGACGTTTTCCACGGCGACA GTTTTAGAGCTAGAAATAGCAAGT
klp-17 3'end	GGAAAAGCAGTTGTTCAAAC GTTTTAGAGCTAGAAATAGCAAGT
klp-12 3'end	GAGATTCGACAGTCGGATTC GTTTTAGAGCTAGAAATAGCAAGT
klp-20 3'end	ATTGCTCACATAACTGGTAC GTTTTAGAGCTAGAAATAGCAAGT
klp-4 3'end	ATCCACCAGGTCTCCTGAAA GTTTTAGAGCTAGAAATAGCAAGT
klp-8 3'end	CAGCGTGCTTAAAGTTCCCA GTTTTAGAGCTAGAAATAGCAAGT

3C Concentrations dsRNAs injected

gene dsRNA targeting	**Concentration (ng/ul)**
mom-2	499
mes-1	441
apr-1	698
mig-5	840
dsh-2	259

Supplemental Table 3 A) Average percent lethality for each strain used in Figures 2 and 5. B) sgRNA primers used generate the Cas9 vector and sgRNA to target each site for gene-specific knock-in. C) Concentrations of double-stranded RNAs injected as measured using a NanoDrop.

Table S4. Observed localization of mNG-fusions

Strain Name	Mammalian gene name	Tag	Localization
LP559	Wnt	MOM-2::mNG	anchor cell
LP184	Frizzled	MOM-5::YPET	seam cells, Q neuroblasts, germ cells, pharynx, unidentified head cells, nerve ring
LP538	Gsk3	GSK-3::mNG	P granules in the early embryo, spindle poles in the early embryo, seam cell, distal tip cell, developing germline, sperm
LP228	Dishevelled	mNG::DSH-2	seam cells, Q neuroblasts, M cells, distal tip cells, ventral midline cells, unidentified head cells
LP728	Dishevelled	mNG-GLO::MIG-5	seam cells, Q neuroblasts, body wall muscles, M cells, distal tip cells, ventral midline cells, unidentified head cells, unidentified tail cells
LP705	Dishevelled	DSH-1:mNG DIX^PDZ	cell conttacts at approximately 100-cell stage, developing germline and vulva, distal tip cells, unidentified head cells, unidentified tail cells, nerve ring, seam cells
LP435	APC	mNG::APR-1	seam cells, Q neuroblasts, distal tip cells, pharynx, ventral midline cells, unidentified head and tail cells
LP713	Axin	PRY-1::mNG	seam cells, and some later embryonic cells
LP530	Ror	CAM-1::mNG	early embryonic cell contacts, seam cells, Q neuroblasts, body wall muscles, pharynx, ventral midline cells, unidentified head cells, sheath cells, nerve ring
LP527	RTK-like	MES-1::mNG	between germcell and endodermal precursor, oocyte cell contacts in the proximal germline
LP563	Dynactin p150	DNC::mNG	divinding cells, early embryonic cell cortex, spindle poles, astral microtubule associated punctea
LP585	NuMA	LIN-5::mNG	divinding cells, early embryonic cell cortex, spindle poles, microtubules, nuclear envelope
LP560	Dynein	DHC::mNG	divinding cells, early embryonic cell cortex, spindle poles, stong nuclear envelope, kinetochore, astral microtubule decoration
LP439	NudE	NUD-2::mNG	chromosomes and DNA in mitotic cells, head neurons, germ cell nucleai
LP451	BicaudalD	mNG::BICD-1	hypodermal cells (comma stage), pharyngeal cells, excluded from developing germline, vulval cells
LP591	Lis1	LIS-1::mNG	early embryonic cell cortex, spindle poles, microtubules, nuclear envelope, diffuse cytoplasm
LP598	Discs large	DLG--1::mNG	apcial cell contacts throughout the developing larva: pharyngeal cells, vulval cells, developing germline
LP447	MCAK	KLP-7::mNG	chromosomes and spindle poles in mitotic cells, distal tip cell, dividing seam cells, unidentified neurons, unidentified tail cells
LP443	Kinesin	KLP-17::mNG	Sperm, developing germline
LP521	Kinesin	KLP-12::mNG	unidentified cells in the developing head
LP608	Kinesin	KLP-20::mNG	puncta in later stage embryos, unidentified anterior neurons, unidentified head cells, distal tip cells
LP600	Kinesin	KLP-4::mNG	Distal tip cell, unspecificed neurons, nerve ring, unidentified head cells
LP604	Kinesin	KLP-8::mNG	broadly distributed puncta in developing larval cells

Supplemental Table 4. Observed localization of mNG-fusions. These data are additional descriptions of where tagged proteins were observed. Note that these data are certain to be incomplete because not every stage was examined for every strain.